



# PACIFIC EARTHQUAKE ENGINEERING RESEARCH CENTER

## **The Rocking Spectrum and the Shortcomings of Design Guidelines**

**Nicos Makris**

Associate Professor

Department of Civil and Environmental Engineering  
University of California, Berkeley

**and**

**Dimitrios Konstantinidis**

Department of Civil and Environmental Engineering  
University of California, Berkeley

# **The Rocking Spectrum and the Shortcomings of Design Guidelines**

**Nicos Makris**

Associate Professor  
Department of Civil and Environmental Engineering  
University of California, Berkeley

and

**Dimitrios Konstantinidis**

Department of Civil and Environmental Engineering  
University of California, Berkeley

PEER Report 2001/07  
Pacific Earthquake Engineering Research Center  
College of Engineering

August 2001

## ABSTRACT

This report is concerned with the superficial similarities and fundamental differences between the oscillatory response of a single-degree-of-freedom (SDOF) oscillator (regular pendulum) and the rocking response of a slender rigid block (inverted pendulum). The study examines the distinct characteristics of the rocking spectrum and compares the observed trends with those of the response spectrum. It is shown that the rocking spectrum complements the response spectrum as an indicator of the shaking potential of earthquakes since it reflects kinematic characteristics of the ground motions that are *not* identifiable by the response spectrum. The study investigates systematically the fundamental differences in the mechanical structure of the two dynamical systems of interest and concludes that rocking structures *cannot* be replaced by “equivalent” single-degree-of-freedom-oscillators. The study proceeds by examining the validity of a simple, approximate design methodology, initially proposed in the late 70’s and now recommended in design guidelines to compute rotations of slender structures by performing iteration either on the true displacement response spectrum or on the design spectrum. This report shows that the abovementioned simple design approach is inherently flawed and should be abandoned, in particular for smaller, less slender blocks. The study concludes that the exact rocking spectrum emerges as a distinct, irreplaceable indicator of the shaking potential of ground motions and should be adopted by the profession as a valuable analysis and design tool.

# TABLE OF CONTENTS

ABSTRACT .....	iii
TABLE OF CONTENTS .....	v
LIST OF FIGURES .....	vii
LIST OF TABLES .....	xi
ACKNOWLEDGEMENTS.....	xiii
CHAPTER 1: INTRODUCTION .....	1
CHAPTER 2: DEFINITIONS, ASSUMPTIONS AND JUSTIFICATIONS .....	5
CHAPTER 3: REVIEW OF THE EARTHQUAKE RESPONSE OF VISCOUSLY DAMPED OSCILLATOR .....	7
CHAPTER 4: REVIEW OF THE ROCKING RESPONSE OF A RIGID BLOCK...	11
CHAPTER 5: ROCKING SPECTRA.....	17
CHAPTER 6: A NEW MEASURE OF EARTHQUAKE SHAKING.....	27
CHAPTER 7: FREE VIBRATIONS OF ROCKING BLOCK .....	31
CHAPTER 8: ESTIMATION OF UPLIFT USING THE RESPONSE SPECTRA....	37
CHAPTER 9: THE FEMA 356 GUIDELINES .....	53
CHAPTER 10: CONCLUSIONS .....	57
REFERENCES .....	59

## LIST OF FIGURES

<b>Figure 1.1</b>	Schematic of a single-degree-of-freedom oscillator (top left) and of a free-standing block in rocking motion (top right); together with the associated force-displacement (bottom left) and moment-rotation (bottom right) diagrams.....	3
<b>Figure 4.1</b>	Rocking response of rigid block: $p=2.0$ rad/sec, $\alpha=15^\circ$ [ $h=1.77$ m, $b=0.48$ m, $R=1.84$ m, $r=0.81$ ], subjected to Type-B pulse with $T_p=2$ sec.....	15
<b>Figure 4.2</b>	Rocking response of rigid block: $p=1.0$ rad/sec, $\alpha=15^\circ$ [ $h=7.11$ m, $b=1.90$ m, $R=7.35$ m, $r=0.81$ m], subjected to Type-B pulse with $T_p=2$ sec.....	16
<b>Figure 5.1</b>	True response spectra of a linear viscously damped oscillator (left) and rocking spectra of a rigid slender block (right) when subjected to the Pacoima Dam motion recorded during the 1971 San Fernando Earthquake. ....	20
<b>Figure 5.2</b>	True response spectra of a linear viscously damped oscillator (left) and rocking spectra of a rigid slender block (right) when subjected to the FN component of the Array #5 motion recorded during the 1979 Imperial Valley earthquake....	21
<b>Figure 5.3</b>	True response spectra of a linear viscously damped oscillator (left) and rocking spectra of a rigid slender block (right) when subjected to the Los Gatos motion recorded during the 1989 Loma Prieta earthquake. ....	22
<b>Figure 5.4</b>	True response spectra of a linear viscously damped oscillator (left) and rocking spectra of a rigid slender block (right) when subjected to the Rinaldi motion recorded during the 1994 Northridge earthquake. ....	23
<b>Figure 5.5</b>	True response spectra of a linear viscously damped oscillator (left) and rocking spectra of a rigid slender block (right) when subjected to the Sylmar motion recorded during the 1994 Northridge earthquake. ....	24
<b>Figure 5.6</b>	True response spectra of a linear viscously damped oscillator (left) and rocking spectra of a rigid slender block (right) when subjected to 1992 Erzinkan, Turkey, earthquake.....	25
<b>Figure 5.7</b>	True response spectra of a linear viscously damped oscillator (left) and rocking spectra of a rigid slender block (right) when subjected to the Takatori motion recorded during the 1995 Kobe, Japan, earthquake. ....	26
<b>Figure 7.1</b>	Equivalent viscous damping, $\beta$ , of a rocking block as results from (a) the Priestley et al. (1978) analogy (Equation 7.9), (light solid lines); (b) the empirical Equation (7.10), (heavy solid lines); and (c) the FEMA 356 formula, (dashed line).....	35
<b>Figure 7.2</b>	Response of SDOF oscillator: $\omega_o=2.0$ rad/sec, $\xi = -0.34 \ln(0.81) = 7.2\%$ , subjected to Type-B pulse with $T_p=2$ sec. ....	36

<b>Figure 8.1</b>	Comparison of exact and approximate uplift spectra (center column) that have been computed with the Priestley et al. (1978) method using the true displacement response spectrum (top left). The converged period that corresponds to the estimated uplift is shown in the right column. Ground Motion: Pacoima Dam, 1971 San Fernando.....	42
<b>Figure 8.2</b>	Selected time histories and durations of rocking cycles of rigid blocks with slenderness, $\alpha=10^\circ$ (left), $\alpha=15^\circ$ (center), and $\alpha=20^\circ$ (right) when subjected to the Pacoima Dam record.....	43
<b>Figure 8.3</b>	Comparison of exact and approximate uplift spectra (center column) that have been computed with the Priestley et al. (1978) method using the true displacement response spectrum (top left). The converged period that corresponds to the estimated uplift is shown in the right column. Ground Motion: El Centro Array #5, 1979 Imperial Valley.....	44
<b>Figure 8.4</b>	Comparison of exact and approximate uplift spectra (center column) that have been computed with the Priestley et al. (1978) method using the true displacement response spectrum (top left). The converged period that corresponds to the estimated uplift is shown in the right column. Ground Motion: Los Gatos, 1989 Loma Prieta.....	45
<b>Figure 8.5</b>	Selected time histories and durations of rocking cycles of rigid blocks with slenderness, $\alpha=10^\circ$ (left), $\alpha=15^\circ$ (center), and $\alpha=20^\circ$ (right) when subjected to the Los Gatos record.....	46
<b>Figure 8.6</b>	Comparison of exact and approximate uplift spectra (center column) that have been computed with the Priestley et al. (1978) method using the true displacement response spectrum (top left). The converged period that corresponds to the estimated uplift is shown in the right column. Ground Motion: Rinaldi, 1994 Northridge.....	47
<b>Figure 8.7</b>	Selected time histories and durations of rocking cycles of rigid blocks with slenderness, $\alpha=10^\circ$ (left), $\alpha=15^\circ$ (center), and $\alpha=20^\circ$ (right) when subjected to the Rinaldi record.....	48
<b>Figure 8.8</b>	Comparison of exact and approximate uplift spectra (center column) that have been computed with the Priestley et al. (1978) method using the true displacement response spectrum (top left). The converged period that corresponds to the estimated uplift is shown in the right column. Ground Motion: Sylmar, 1994 Northridge.....	49
<b>Figure 8.9</b>	Selected time histories and durations of rocking cycles of rigid blocks with slenderness, $\alpha=10^\circ$ (left), $\alpha=15^\circ$ (center), and $\alpha=20^\circ$ (right) when subjected to the Sylmar record.....	50
<b>Figure 8.10</b>	Comparison of exact and approximate uplift spectra (center column) that have been computed with the Priestley et al. (1978) method using the true displacement response spectrum (top left). The converged period that	

	corresponds to the estimated uplift is shown in the right column. Ground Motion: 1992 Erzinkan, Turkey.....	51
<b>Figure 8.11</b>	Comparison of exact and approximate uplift spectra (center column) that have been computed with the Priestley et al. (1978) method using the true displacement response spectrum (top left). The converged period that corresponds to the estimated uplift is shown in the right column. Ground Motion: Takatori, 1995 Kobe, Japan.....	52
<b>Figure 9.1</b>	Comparison of exact and design uplift spectra that have been computed with the Priestley et al. (1978) method using the FEMA design displacement spectra. When the solid line is not shown, the FEMA procedure predicts overturning over the entire $2\pi/p$ range shown. ....	55
<b>Figure 9.2</b>	Comparison of exact and design uplift spectra that have been computed with the Priestley et al. (1978) method using the FEMA design displacement spectra. When the solid line is not shown, the FEMA procedure predicts overturning over the entire $2\pi/p$ range shown. ....	56

## LIST OF TABLES

<b>Table 3.1</b>	Parameters Used to Construct the FEMA Acceleration Design Spectra.....	8
<b>Table 5.1</b>	Peak Ground Accelerations (PGA), Peak Ground Velocities (PGV) and Approximate Main Pulse Periods of Selected Earthquake Motions Next to Values of Block-Slenderness of Interest.....	18
<b>Table 5.2</b>	Selective Characteristics and Parameters of the Two One-Degree-of- Freedom Systems of Interest.....	19

## **ACKNOWLEDGEMENTS**

This work was conducted during a one-semester-long sabbatical leave of the senior author from the University of California at Berkeley. Partial financial support for this study was provided by the Pacific Gas and Electric Company under Grant PG&E-UCB-0095 and by Simpson Gumpertz & Heger Inc., Consulting Engineers.

This work made use of Pacific Earthquake Engineering Research Center shared facilities supported by the Earthquake Engineering Research Center Program of the National Science Foundation under award number EEC-9701568.

# 1 Introduction

Reconnaissance reports following strong earthquakes include the rocking and overturning of a variety of slender structures such as electrical equipment, retaining walls, liquid storage tanks, tall rigid buildings, and tombstones. The need to understand and predict these failures in association with the temptation to estimate levels of ground motion by examining whether slender structures have overturned or survived the earthquakes has motivated a number of studies on the rocking response of rigid blocks (Milne 1885, Housner 1963, Yim et al. 1980, Hogan 1989, Shenton 1996, Makris and Roussos 2000, Zhang and Makris 2001, among others, and references reported therein).

The first systematic study on the dynamic response of a rigid yet slender block supported on a base undergoing horizontal acceleration was presented by Housner (1963), who examined the free- and forced-vibration responses to rectangular and half-sine pulse excitations. Using an energy approach, he presented an approximate analysis of the dynamics of a rigid block subjected to a white-noise excitation, uncovering a scale effect that explained why the larger of two geometrically similar blocks could survive the excitation, while the smaller block topples.

The publication of Housner's paper in association with the realistic possibility that building structures may uplift and rock during seismic loading motivated further studies on the seismic response of structures free to rock on their foundations. Priestley et al. (1978) presented early experimental studies on a slender model structure in an attempt to (a) validate some of

Housner's (1963) theoretical results and (b) to develop a practical methodology to compute displacements of the center of gravity of the structure due to rocking motion by using standard displacement and acceleration response spectra. Unfortunately, the Priestley et al. study is based on the sweeping—and, as will be shown, erroneous—assumption that “*it is possible to represent a rocking block as a single-degree-of-freedom oscillator with constant damping, whose period depends on the amplitude of rocking.*” The unsubstantiated analogies and oversimplified methodologies proposed in the Priestley et al. (1978) paper are revisited herein in depth, since they have been adopted without sufficient scrutiny by the FEMA 356 document: *Prestandard and Commentary for the Seismic Rehabilitation of Buildings*.

Figure 1.1 (top) shows the schematic of the two SDOF structures at their deformed configurations when subjected to ground shaking. The response quantities of interest for the SDOF oscillator are its relative displacement,  $u$ , and its time derivatives. The corresponding quantities of interest for the rocking block are its rotation,  $\theta$ , and its first time derivative—that is the angular velocity,  $\dot{\theta}$ . In parallel to the response spectra, the report advances the concept of the rocking spectra which are plots of the maximum rotation,  $\theta$ , and maximum angular velocity,  $\dot{\theta}$ , versus the frequency parameter (or its inverse) of geometrically similar blocks (with same width-to-height ratio). Rocking spectra can be used directly to estimate the uplift or overturning of a variety of structures that tend to engage into rocking motion, ranging from tombstones to stiff bridge towers. The report shows that the rocking spectrum is a distinct and valuable indicator of the shaking potential of earthquakes and offers information on the earthquake shaking that is not identifiable by the response spectrum.

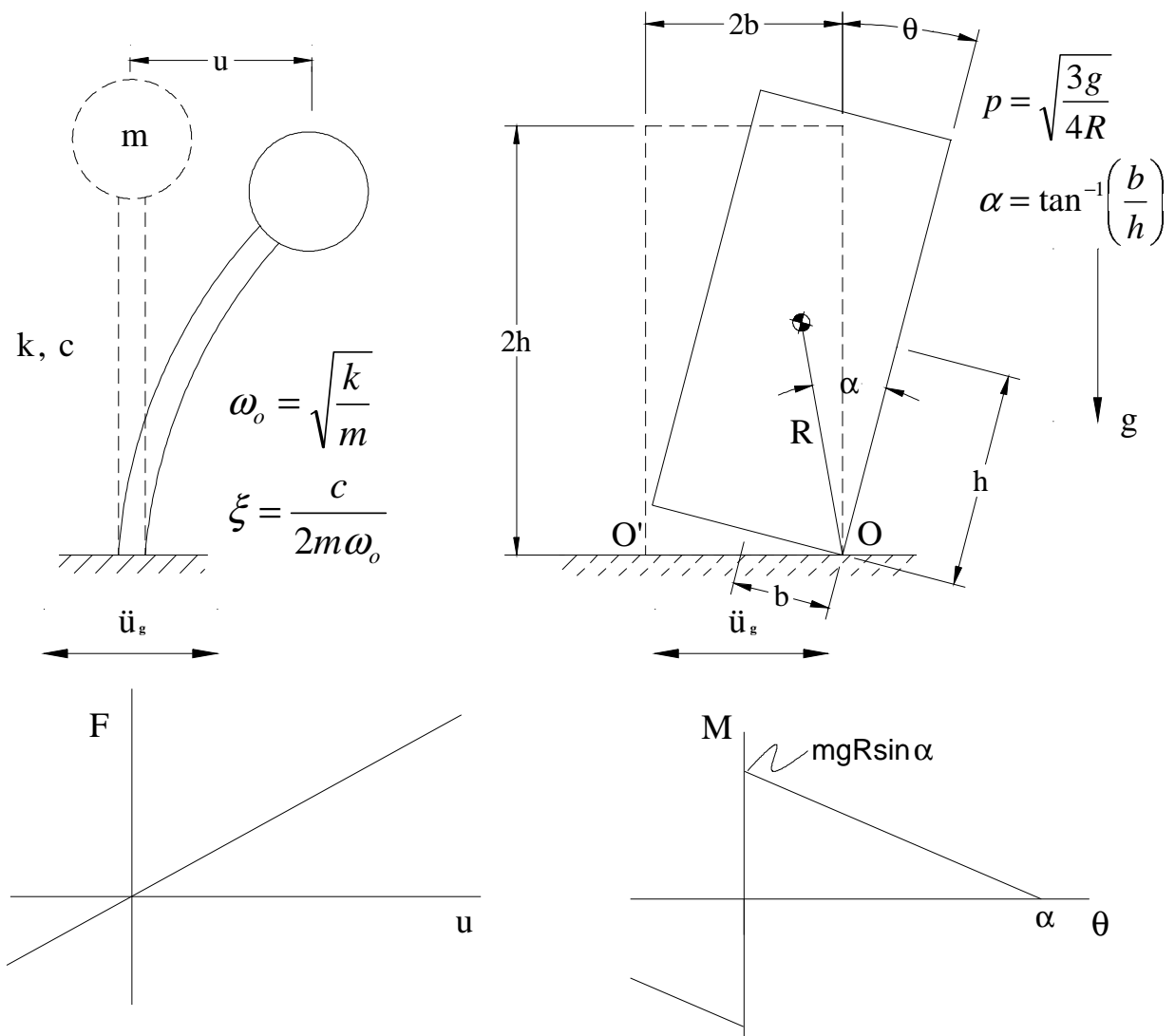


**Figure 1.1** Schematic of a single-degree-of-freedom oscillator (top left) and of a free-standing block in rocking motion (top right); together with the associated force-displacement (bottom left) and moment-rotation (bottom right) diagrams.

## 2 Definitions, Assumptions, and Justifications

In this study, the term *oscillations* is used solely for the response of the linear single-degree-of-freedom oscillator, whereas the term *vibrations* is used for the rocking response of a rigid block. This subtle distinction is introduced to differentiate between the free-vibration response of the SDOF oscillator that is described by *trigonometric* functions and the solution of the linearized equations that govern the free-vibration response of a rocking block that is described by *hyperbolic* functions.

When a rigid block is rocking, it is assumed that the rotation continues smoothly from point O to O'. This constraint in association with conservation of momentum requires an energy loss during impact that emerges from the requirement that the block sustains rocking motion. The energy loss during impact depends on the slenderness of the block. An energy loss during impact that is greater than the minimum energy loss required for the realization of rocking motion will result in more rapid decay of the vibrations. Conversely, an energy loss during impact that is less than the aforementioned minimum energy loss will induce a lift that distorts the pure rocking assumption. The finite energy loss during impact results in an instantaneous reduction of the angular velocity when the rotation reverses—therefore, in theory, the angular velocity history is non-differentiable. In reality, during impact, there is a local plastic deformation at the pivot point that results in large but finite angular accelerations, which are not

computed in this analysis. Regardless of what the exact value of the angular acceleration is, the existence of rocking motion is inherently associated with damping. Hence the rocking response of a rigid block is compared with the oscillatory response of a *damped oscillator*. In this study, we focus on the viscously damped oscillator, although other damping mechanisms could be assumed without difficulty. Within the context of constitutive relations, the restoring mechanism of the SDOF oscillator originates from the elasticity of the structure, while the restoring mechanism of the rocking block originates from gravity. Figure 1.1 (bottom) shows the force-displacement and moment-rotation relations of the two elementary structures of interest. Some of the fundamental differences in the mechanical structure of these two systems become apparent. The SDOF oscillator has a positive and finite stiffness,  $k$ , and energy is dissipated as the force-displacement curve forms closed loops. In contrast, the rocking block has infinite stiffness until the magnitude of the applied moment reaches  $mgR\sin\alpha$ , and once the block is rocking, its stiffness assumes a negative value and decreases monotonically, reaching zero when  $\theta=\alpha$ =block slenderness.

### 3 Review of the Earthquake Response of Viscously Damped Oscillator

The dynamic equilibrium of the mass,  $m$ , shown at the top left of Figure 1.1 gives

$$m\ddot{u}(t) + c\dot{u}(t) + ku(t) = -m\ddot{u}_g(t) \quad (3.1)$$

where  $c$  and  $k$  are the damping and stiffness constants, and  $\ddot{u}_g$  is the ground-induced horizontal acceleration. Using the standard notation  $k=m\omega_o^2$  and  $c=2\xi m\omega_o$ , where  $\omega_o=2\pi/T_o$  is the undamped natural frequency, and  $\xi$  is the damping ratio, Equation (3.1) becomes

$$\ddot{u}(t) + 2\xi\omega_o\dot{u}(t) + \omega_o^2u(t) = -\ddot{u}_g(t) \quad (3.2)$$

Equation (3.1), or (3.2), and its solution have been treated in several books of structural dynamics (Chopra 2000, Clough and Penzien 1993, among others). Alternatively, the solution of Equation (3-2) can be computed with a state-space formulation, where the state vector of the system is merely

$$\{y(t)\} = \begin{Bmatrix} u(t) \\ \dot{u}(t) \end{Bmatrix} \quad (3.3)$$

and the time derivative vector is

$$\{f(t)\} = \begin{Bmatrix} \dot{u}(t) \\ -2\xi\omega_o\dot{u}(t) - \omega_o^2u(t) - \ddot{u}_g(t) \end{Bmatrix} \quad (3.4)$$

The integration of Equation (3.2), or (3.4), yields the earthquake response of the SDOF oscillator. Traditionally, it has been presented in terms of response maxima as a function of the fundamental period of the oscillator,  $T_o = 2\pi/\omega_o$ , and the damping ratio,  $\xi = c/(2m\omega_o)$ .

Figure 5.1 (left) plots the true displacement, velocity, and acceleration spectra of the linear, viscously damped oscillator for values of damping  $\xi = 5\%$ ,  $10\%$ , and  $15\%$ , subjected to the fault-normal component of the Pacoima Dam motion recorded during the 1971 San Fernando earthquake. The bottom-left graph also shows the  $\xi = 5\%$  UBC97 (type-D soil is assumed for all UBC spectra in this report) and FEMA 356 acceleration design spectra tailored for the specific site. Table 3.1 shows the parameters used to construct the FEMA 356 design acceleration spectra for the U.S. ground motions appearing in this study. The reference acceleration values of  $S_{xs}$  and  $S_{xl}$  that define the shape of the design spectrum are obtained by modifying the mapped  $S_s$  and  $S_l$  values for the appropriate site class.

**Table 3.1** Parameters Used to Construct the FEMA Design Acceleration Spectra

Ground Motion	Site Class	$S_{xs}$ (g)	$S_{xl}$ (g)
San Fernando, 1971 Pacoima Dam	B	1.59	0.50
Imperial Valley, 1979 El Centro #5	D	1.34	0.81
Loma Prieta, 1989 Los Gatos	D	1.94	1.83
Northridge, 1994 Rinaldi FN	C	1.56	0.69
Northridge, 1994 Sylmar FN	D	1.56	0.80

The FEMA design displacement spectra shown in the top-left graphs of Figures 5.1 to 5.5 are computed with the design formula

$$S_d = S_a g \frac{T_o^2}{4\pi^2} \quad (3.5)$$

as recommended in Chapter 4, *Foundations and Geologic Site Hazards*, of the FEMA 356 document. Clearly, the spectral displacement values resulting from Equation (3.5) do not converge at long periods to the actual peak ground displacements. In contrast, the true displacement spectra shown in the top left of Figure 5.1 initially increase with the structural period and eventually converge to the peak ground displacement. Similar trends are observed in Figures 5.2 to 5.7 that plot true response spectra for other major historic earthquakes.

## 4 Review of the Rocking Response of a Rigid Block

We consider the rigid block shown on the right of Figure 1.1. The block can pivot about the centers of rotation  $O$  and  $O'$  when it is set to rocking. Depending on the level and form of the ground acceleration, the block may translate with the ground, slide, rock, or slide-rock. Before 1996, the mode of rigid body motion that prevailed was determined by comparing the available static friction to the width-to-height ratio of the block, irrespective of the magnitude of the horizontal ground acceleration. Shenton (1996) indicated that in addition to pure sliding and pure rocking, there is a slide-rock mode, and its manifestation depends not only on the width-to-height ratio and the static friction coefficient, but also on the magnitude of the base acceleration.

Assuming that the coefficient of friction is large enough so that there is no sliding, under a positive horizontal acceleration that is sufficiently large, a rigid block will initially rotate with a negative rotation,  $\theta < 0$ , and, if it does not overturn, it will eventually assume a positive rotation; and so on.

The equations that govern the rocking motion under a horizontal ground acceleration  $\ddot{u}_g(t)$  are

$$I_o \ddot{\theta}(t) + mgR \sin(-\alpha - \theta) = -m\ddot{u}_g(t)R \cos(-\alpha - \theta), \quad \theta < 0 \quad (4.1)$$

and

$$I_o \ddot{\theta}(t) + mgR \sin(\alpha - \theta) = -m\ddot{u}_g(t)R \cos(\alpha - \theta), \quad \theta > 0 \quad (4.2)$$

where  $I_o$  is the moment of inertia of the rigid block. Equations (4.1) and (4.2) are well known in the literature (Yim et al. 1980, Makris and Roussos 2000, among others) and are valid for arbitrary values of the angle  $\alpha = \tan^{-1}(b/h)$ . For rectangular blocks,  $I_o = \frac{4}{3}mR^2$ , Equations (4.1) and (4.2) can be expressed in the compact form

$$\ddot{\theta}(t) = -p^2 \left\{ \sin[\alpha \operatorname{sgn}[\theta(t)] - \theta(t)] + \frac{\ddot{u}_g}{g} \cos[\alpha \operatorname{sgn}[\theta(t)] - \theta(t)] \right\} \quad (4.3)$$

where  $p = \sqrt{3g/(4R)}$  is the *frequency parameter* of a rectangular block. The larger the block (larger  $R$ ), the smaller  $p$ . The vibration frequency of a rigid block under free vibration is not constant since it depends on the vibration amplitude (Housner 1963). Nevertheless, when two geometrically similar blocks (same  $\alpha$ ) of different size (different  $p$ ) experience free vibrations with the same initial conditions,  $\theta_o$  and  $\dot{\theta}_o = 0$ , each response-cycle of the larger block (smaller  $p$ ) is longer than the corresponding response-cycle of the smaller block (larger  $p$ ). Accordingly, the quantity  $p$  is a measure of the dynamic characteristic of the block. It depends on the size of the block,  $R$ , and the intensity of the gravitational field,  $g$ . The solution of Equation (4.3) is obtained numerically via a state-space formulation where the state vector of the system is

$$\{y(t)\} = \begin{Bmatrix} \theta(t) \\ \dot{\theta}(t) \end{Bmatrix} \quad (4.4)$$

and the time-derivative vector  $f(t)$  is

$$\{f(t)\} = \{\dot{y}(t)\} = \begin{Bmatrix} \dot{\theta}(t) \\ -p^2 \left\{ \sin[\alpha \operatorname{sgn}[\theta(t)] - \theta(t)] + \frac{\ddot{u}_g}{g} \cos[\alpha \operatorname{sgn}[\theta(t)] - \theta(t)] \right\} \end{Bmatrix} \quad (4.5)$$

The numerical integration of (4.5) and (3.4) is performed with standard ODE solvers available in MATLAB (1999). The solution of (4.5) is constructed by accounting for the energy loss at every impact. When the angle of rotation reverses, it is assumed that the rotation continues smoothly

from point O to O'. Conservation of momentum about point O' just before the impact and immediately after the impact gives (Housner 1963)

$$I_o \dot{\theta}_1 - m \theta_1 2bR \sin \alpha = I_o \dot{\theta}_2 \quad (4.6)$$

where  $\dot{\theta}_1$  is the angular velocity just prior to the impact, and  $\dot{\theta}_2$  is the angular velocity right after the impact. The ratio of the kinetic energy after and before the impact is

$$r = \frac{\dot{\theta}_2^2}{\dot{\theta}_1^2} \quad (4.7)$$

which means that the angular velocity after the impact is only  $\sqrt{r}$  times the velocity before the impact. Substitution of (4.7) into (4.6) gives

$$r = \left[ 1 - \frac{3}{2} \sin^2(\alpha) \right]^2 \quad (4.8)$$

The value of the coefficient of restitution given by (4.8) is the maximum value of  $r$  under which a block with slenderness  $\alpha$  will undergo rocking motion. Consequently, in order to observe rocking motion, the impact has to be inelastic. The less slender a block (larger  $\alpha$ ), the more energy has to be lost during impact in order to observe rocking motion. Therefore, the slenderness of a rocking block is a measure of the minimum damping of the system.

The integration of (4.5) in association with the constraint expressed by (4.6) yields time histories of the rotation and angular velocities. Figure 4.1 shows the computed rotation and angular velocity histories of a rigid block with frequency parameter  $p=2.0$  rad/sec ( $2\pi/p=3.14$  sec) and slenderness  $\alpha=15^\circ$  [ $h=1.78\text{m}$  (70"),  $b=0.48\text{m}$  (18.76"),  $r=0.81$ ] subjected to three different levels of a 2-sec-long one-cosine (Type-B) pulse (Makris and Roussos 2000).

$$\ddot{u}_g(t) = a_p \cos(\omega_p t), \quad 0 \leq t \leq T_p, \quad (4.9)$$

where  $T_p = 2\pi / \omega_p$  is the period and duration of the pulse. The left column of Figure 4.1 shows the block response when  $a_p=0.310g$ . Following the expiration of the pulse, the block experiences more than 20 impacts within the 8 subsequent seconds. The center column of Figure 4.1 shows the block response on the verge of overturning. Note that just a 1.6% increase in the acceleration amplitude of the excitation pulse alters drastically the response that exhibits only 7 impacts within the 8 subsequent seconds. The right column of Figure 4.1 shows the block response when it overturns, which happens for an acceleration amplitude  $a_p=0.316g$ . Note that when the block does not overturn (left and center columns), the frequency of vibration during the free-vibration regime increases as the rotation amplitude decreases.

Figure 4.2 shows the rotation and angular velocity histories of a rigid block with frequency parameter  $p=1.0$  rad/sec ( $2\pi/p=6.28$  sec) and slenderness  $\alpha=15^\circ$ —that is the same as the slenderness of the smaller block of Figure 4.1—subjected to three levels of a 2-sec-long one-cosine pulse. The amplitude of the excitation pulse in the first column,  $a_p=0.410g$  is tuned so that the peak rotation of the larger block ( $p=1.0$  rad/sec) after the expiration of the pulse is  $\theta/\alpha=0.38$ , which is *equal* to the peak rotation of the smaller block ( $p=2.0$  rad/sec—see Figure 4.1) that happens after the expiration of the 2-sec-long pulse. In comparing Figures 4.1 and 4.2, one observes that while the two different size blocks with same slenderness  $\alpha=15^\circ$  experience free vibrations with the same initial conditions ( $\theta/\alpha=0.38$ ,  $\dot{\theta}=0$ ), each vibration period of the larger block ( $p=1.0$  rad/sec) is longer than the corresponding vibration period of the smaller block. The center and right columns of Figure 4.2 plot the response of the large block on the verge of overturning.

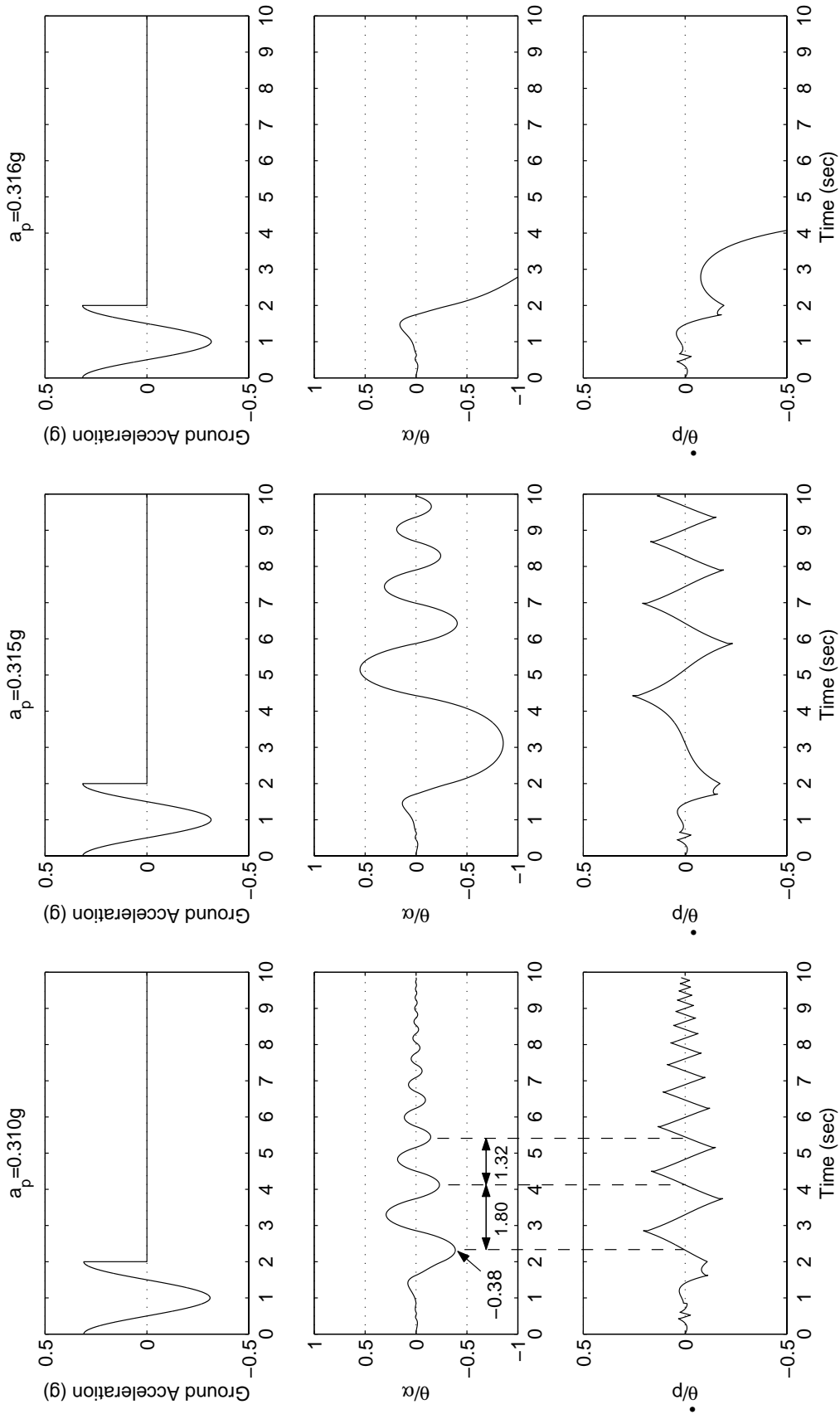


**Figure 4.1** Rocking response of rigid block:  $p=2.0$  rad/sec,  $\alpha=15^\circ$  [ $h=1.77$  m,  $b=0.48$  m,  $R=1.84$  m,  $r=0.81$ ], subjected to Type-B pulse with  $T_p = 2$  sec.

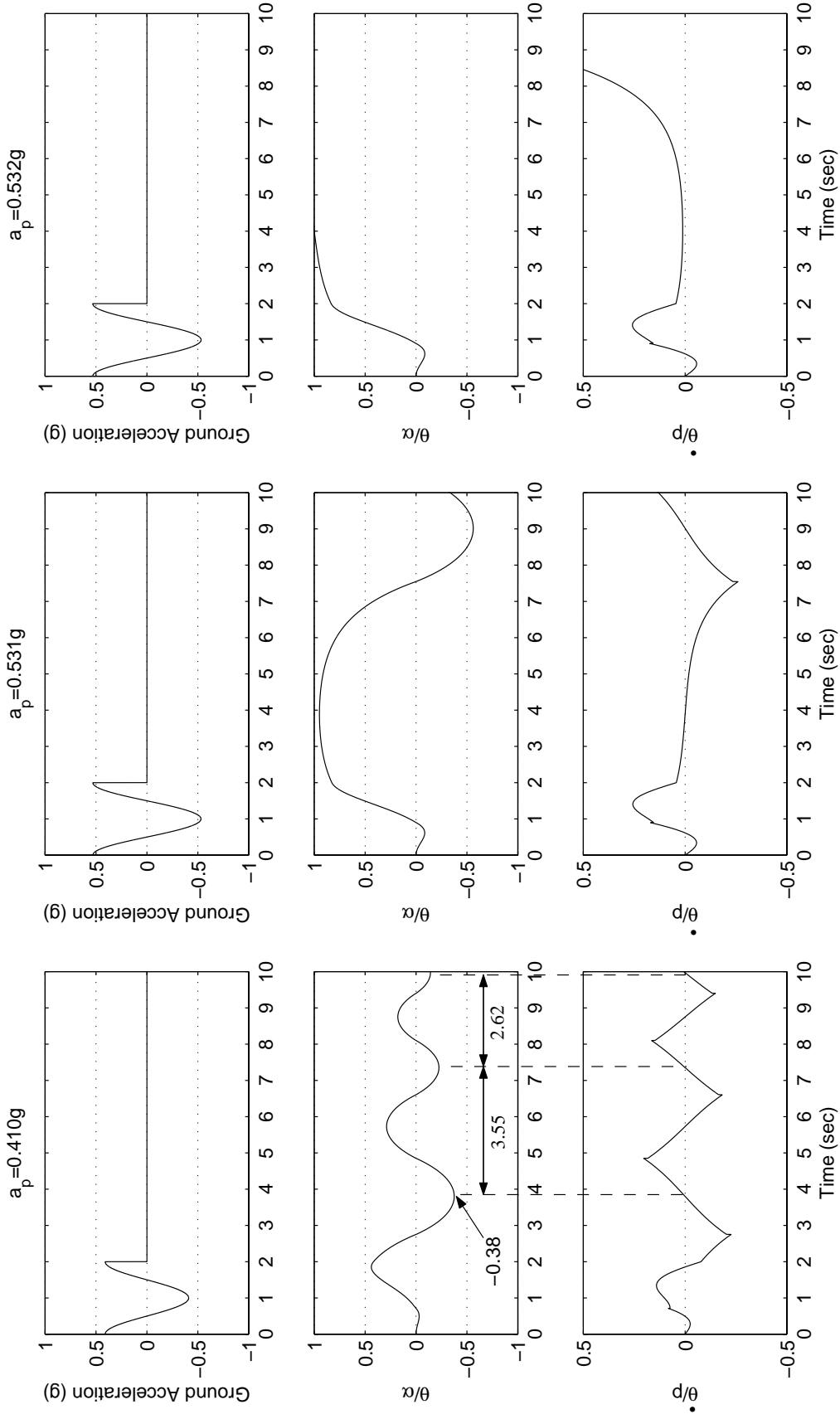


**Figure 4.2** Rocking response of rigid block:  $p=1.0$  rad/sec,  $\alpha=15^\circ$  [ $h=7.11$  m,  $b=1.90$  m,  $R=7.35$  m,  $r=0.81$  m], subjected to Type-B pulse with  $T_p=2$  sec.

## 5 Rocking Spectra

Parallel to the response spectra, one can generate rotation and angular velocity spectra (rocking spectra) as a function of the “period”  $T=2\pi/p$  and different values of slenderness (damping),  $\alpha = \tan^{-1}(b/h)$ . The minimum ground acceleration needed to initiate rocking can be computed from static analysis, which yields that  $\ddot{u}_g/g \geq \tan(\alpha)$ . Table 5.1 offers the peak ground acceleration (PGA) of the strong-motion records used in this study together with the values of  $\tan(\alpha)$  for the range of slenderness that is of interest. For instance, the El Centro Array #5 record with  $\text{PGA}/g=0.379$  can barely induce uplift to a block with slenderness  $\alpha=20^\circ$  ( $\tan(\alpha)=0.364$ ); however, it will not be able to uplift a block with  $\alpha=21^\circ$  since  $\tan(21^\circ)=0.384 > 0.379 = \text{PGA}/g$ . Next to the peak ground accelerations, Table 5.1 offers the peak ground velocities of the ground motions together with the duration of main pulses that can be identified within most of these main near-source ground motions (Makris and Roussos 2000). These kinematic characteristics of the ground are used later in this section where observations from response spectra and rocking spectra are discussed.

The right side of Figures 5.1 to 5.7 plots rotation and angular velocity spectra next to the displacement and velocity spectra presented earlier. As  $2\pi/p$  increases, one moves to larger blocks. Larger values of the slenderness  $\alpha$  correspond to larger amount of energy lost during impact. The most striking observation is that the displacements of oscillating structures, increase

as the natural period  $T_o=2\pi/\omega_o$  increases, reach a maximum, and subsequently converge to the ground displacement; whereas the rotations of rocking structures decrease nearly monotonically as their apparent “period”  $T=2\pi/p$  increases. This known behavior—that larger blocks (longer-period structures) experience smaller rotations than smaller blocks (Housner 1963)—has not been adopted by the profession to the extent that it deserves. For instance, in many occasions there have been attempts to estimate the response of rocking structures by borrowing results from the response of oscillating structures and their associated displacement response spectra that amplify along certain period ranges with a pattern that is drastically different from the pattern

**Table 5.1** Peak Ground Accelerations (PGA), Peak Ground Velocities (PGV) and Approximate Main Pulse Periods of Selected Earthquake Motions Next to Values of Block-Slenderness of Interest.

Ground Motion	PGA/g	PGV (m/sec)	Approximate Value of Main Pulse Period, $T_p$ (sec)	Slenderness ( $\alpha$ )	$\tan(\alpha)$
San Fernando, 1971 Pacoima Dam	1.226	1.20	1.3	$10^\circ=0.175\text{rad}$	0.176
Imperial Valley, 1979 El Centro #5	0.379	0.90	3.2	$12^\circ=0.209\text{rad}$	0.212
Loma Prieta, 1989 Los Gatos	0.563	0.95	3.0	$15^\circ=0.262\text{rad}$	0.268
Northridge, 1994 Rinaldi FN	0.838	1.75	1.0	$17^\circ=0.175\text{rad}$	0.306
Northridge, 1994 Sylmar FN	0.732	1.20	2.3	$20^\circ=0.349\text{rad}$	0.364
Turkey, 1992 Erzinkan	0.515	0.70	1.8	$22^\circ=0.384\text{rad}$	0.404
Kobe, 1995 Takatori	0.611	1.25	-	$25^\circ=0.436\text{rad}$	0.466

that rotation spectra follow. In addition to the different trends observed in the spectra of the SDOF oscillator and the rocking block, Table 5.2 summarizes selective characteristics and parameters that emerge from the two systems of interest and identifies some of the fundamental differences in their dynamical structure. In view of these inherent differences, any analogy between the responses of the two systems tends to be superficial.

**Table 5.2** Selective Characteristics and Parameters of the Two One-Degree-of-Freedom Systems of Interest.

<b>PARAMETERS/ CHARACTERISTICS</b>	<b>Damped Oscillator <i>m, c, k</i></b>	<b>Rocking Rigid Block <i>b, h, g</i></b>
<i>Restoring Mechanism</i>	Elasticity of the structure	Gravity
<i>Restoring force/moment</i>	$F = ku$ (for linear springs)	$M = mgR \sin(\alpha - \theta)$ $R = \sqrt{b^2 + h^2}$
<i>Stiffness at stable equilibrium</i>	Finite	Infinite
<i>Restoring force/moment at stable equilibrium</i>	Zero	Finite: $mgR \sin(\alpha)$
<i>Stiffness away from equilibrium</i>	Positive	Negative
<i>Frequency parameter</i>	Undamped natural frequency: $\omega_o = \frac{2\pi}{T_o} = \sqrt{\frac{k}{m}}$	Frequency Parameter: $p = \sqrt{\frac{3g}{4R}}$ (for rectangular blocks)
<i>Damping Parameter</i>	Viscous damping ratio: $\xi = \frac{c}{2m\omega_o}$	Slenderness: $\alpha = \tan^{-1}(b/h)$

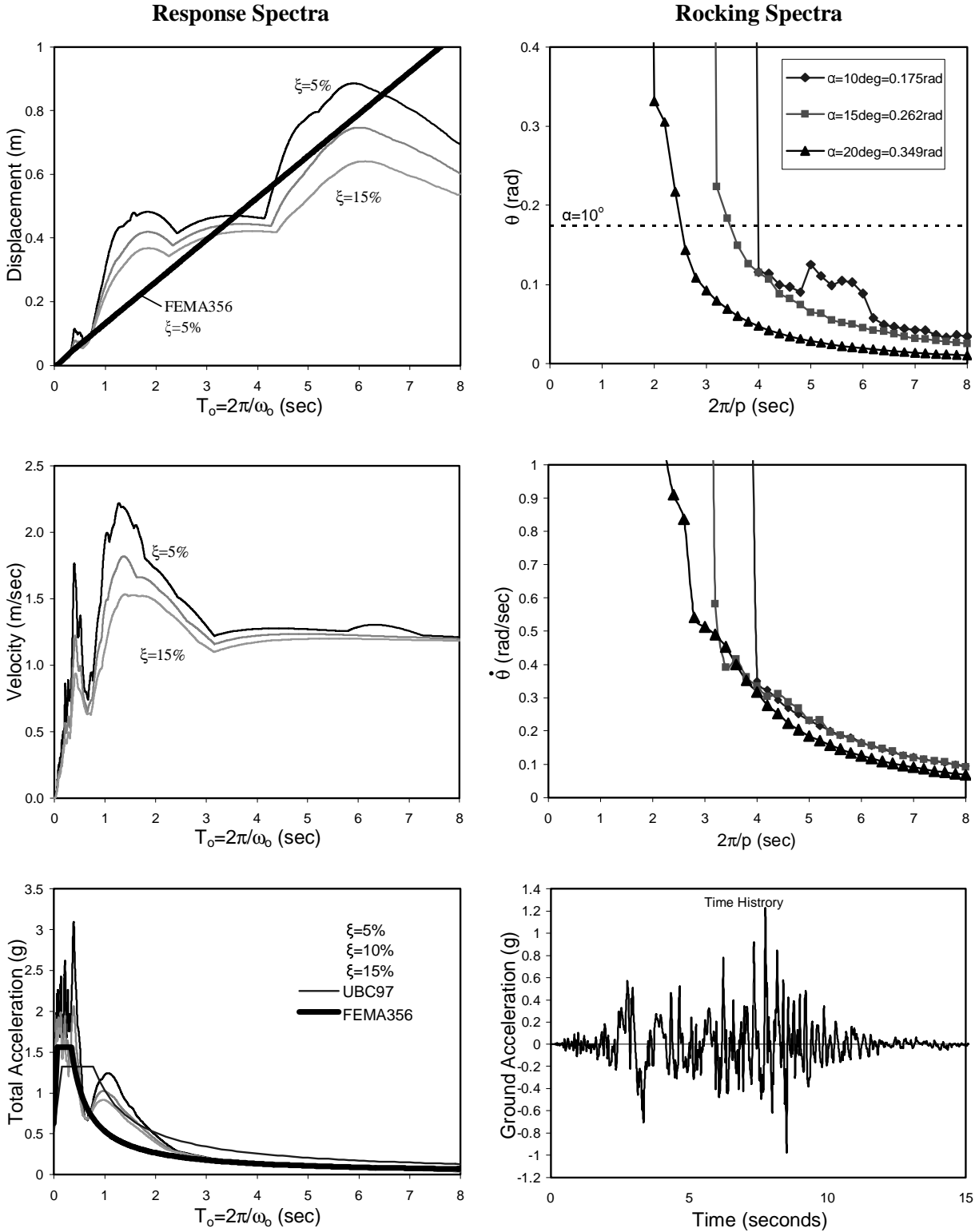


**Figure 5.1** True response spectra of a linear viscously damped oscillator (left) and rocking spectra of a rigid slender block (right) when subjected to the Pacoima Dam motion recorded during the 1971 San Fernando Earthquake.

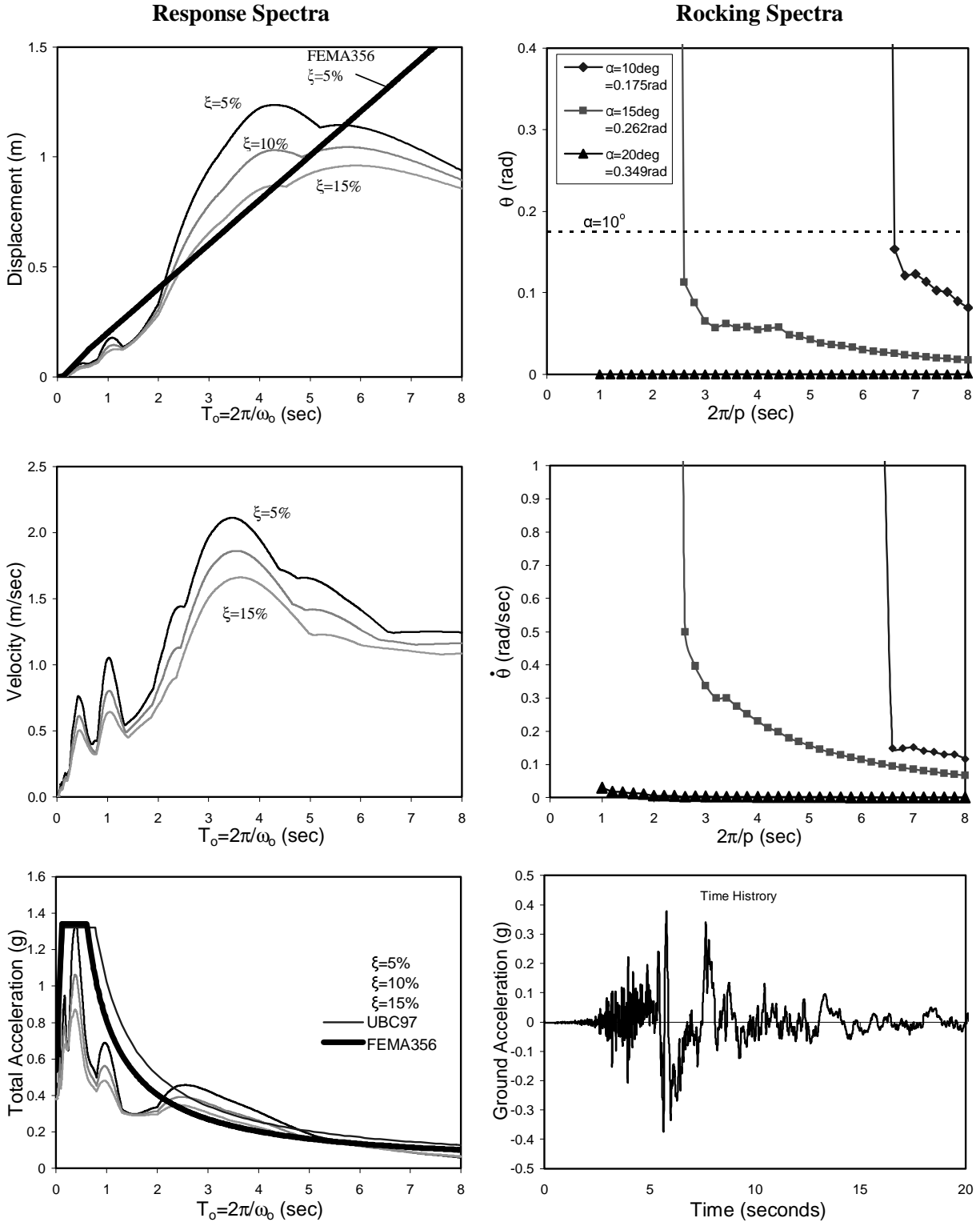


**Figure 5.2** True response spectra of a linear viscously damped oscillator (left) and rocking spectra of a rigid slender block (right) when subjected to the FN component of the Array #5 motion recorded during the 1979 Imperial Valley earthquake.

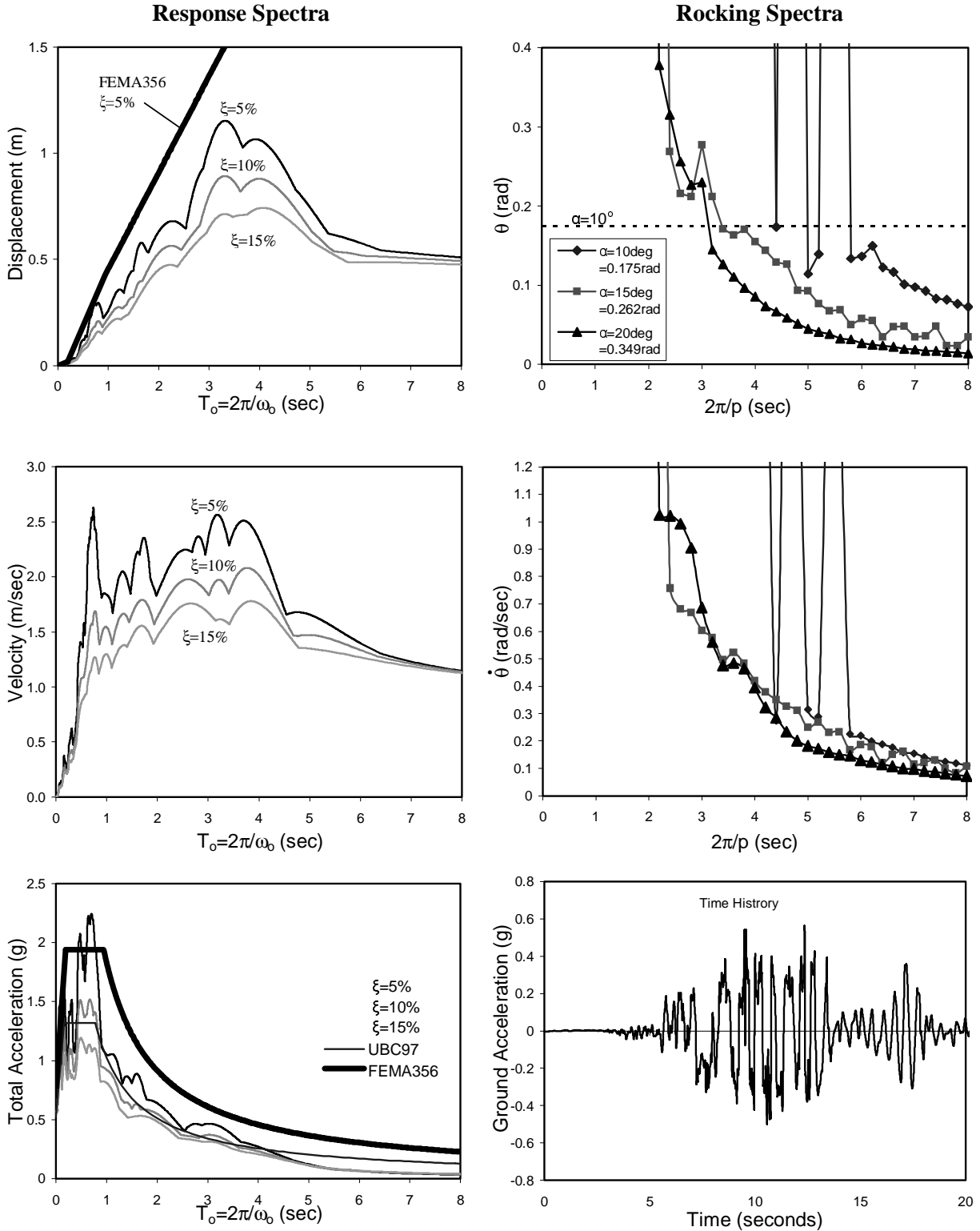


**Figure 5.3** True response spectra of a linear viscously damped oscillator (left) and rocking spectra of a rigid slender block (right) when subjected to the Los Gatos motion recorded during the 1989 Loma Prieta earthquake.

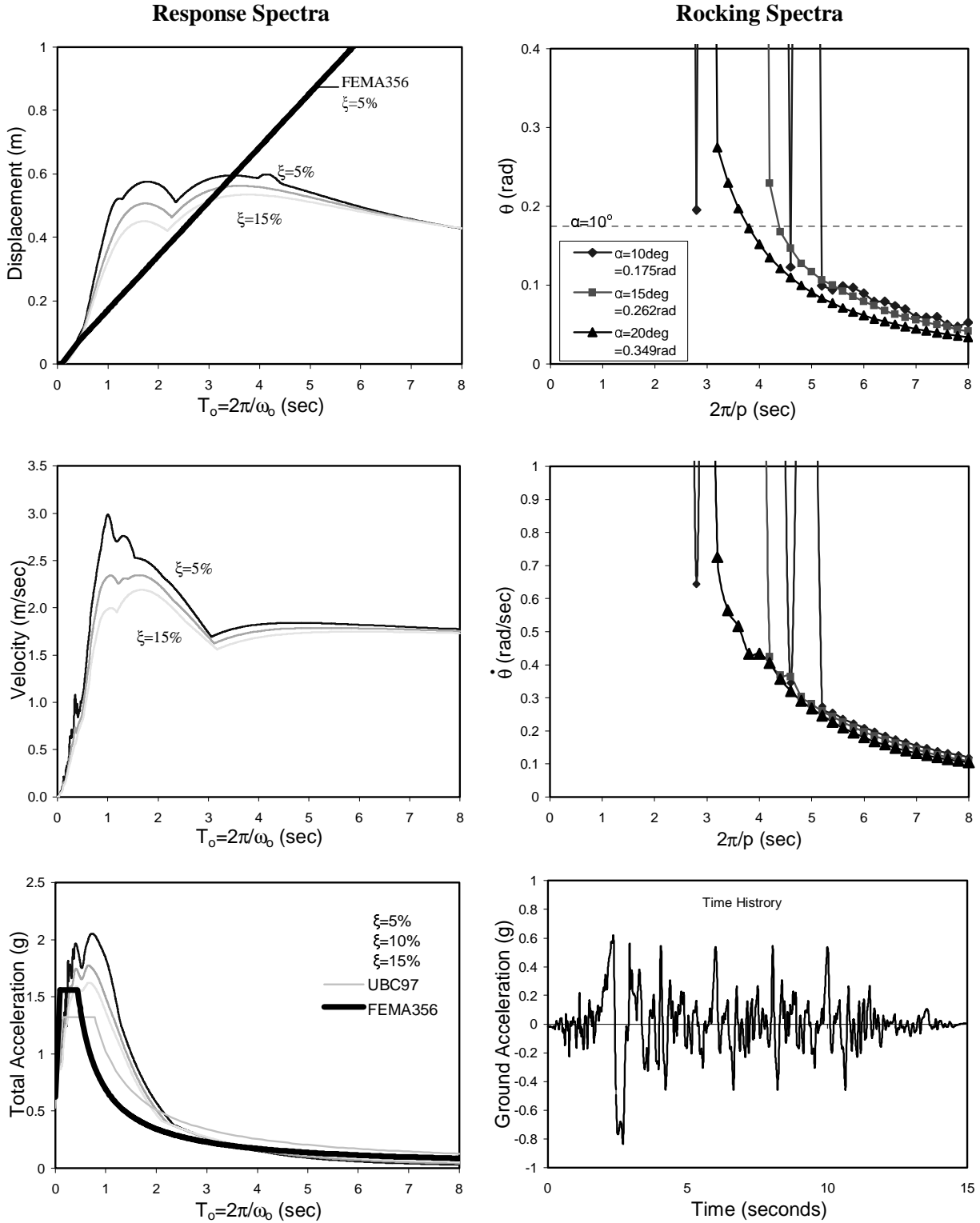


**Figure 5.4** True response spectra of a linear viscously damped oscillator (left) and rocking spectra of a rigid slender block (right) when subjected to the Rinaldi motion recorded during the 1994 Northridge earthquake.

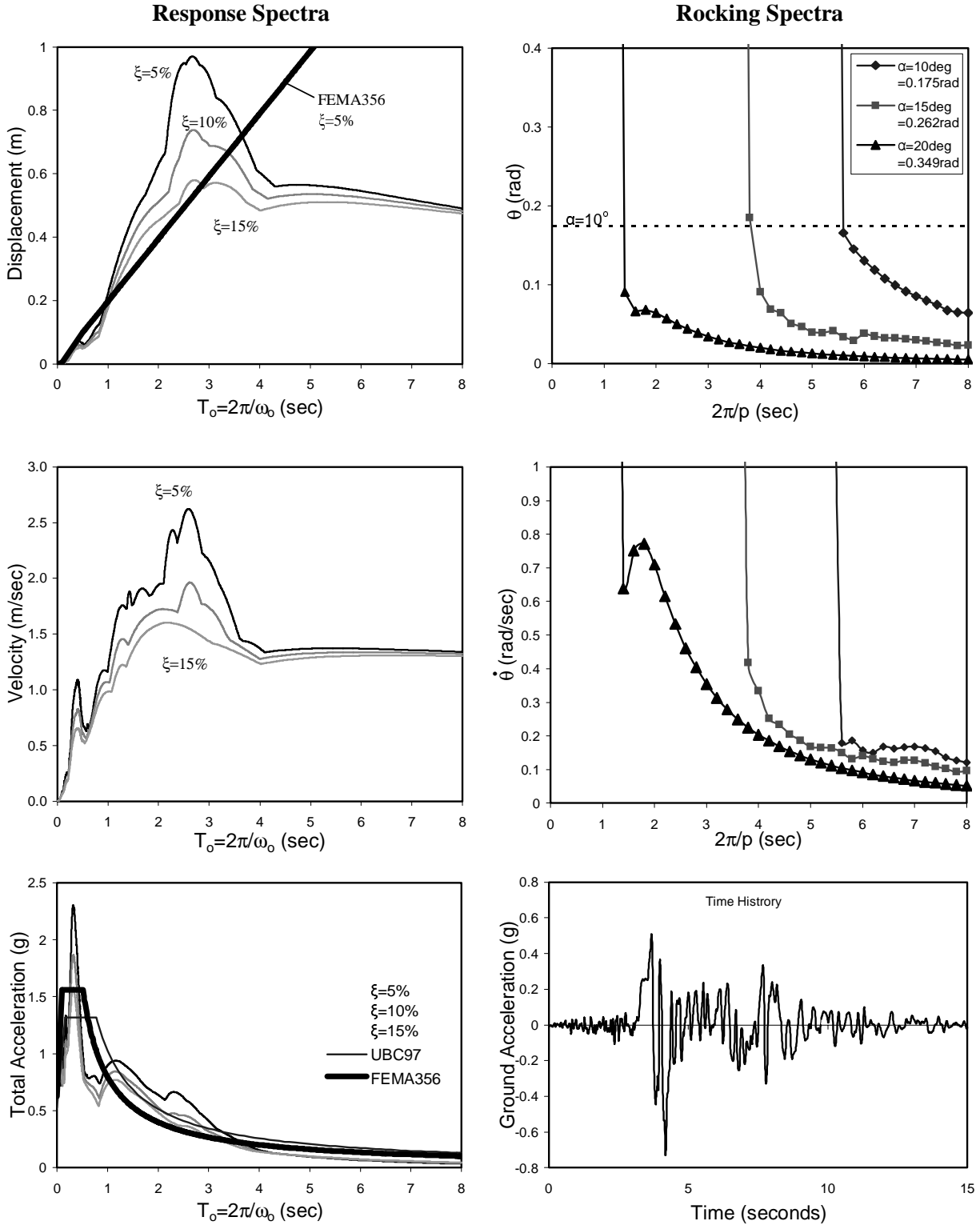


**Figure 5.5** True response spectra of a linear viscously damped oscillator (left) and rocking spectra of a rigid slender block (right) when subjected to the Sylmar motion recorded during the 1994 Northridge earthquake.

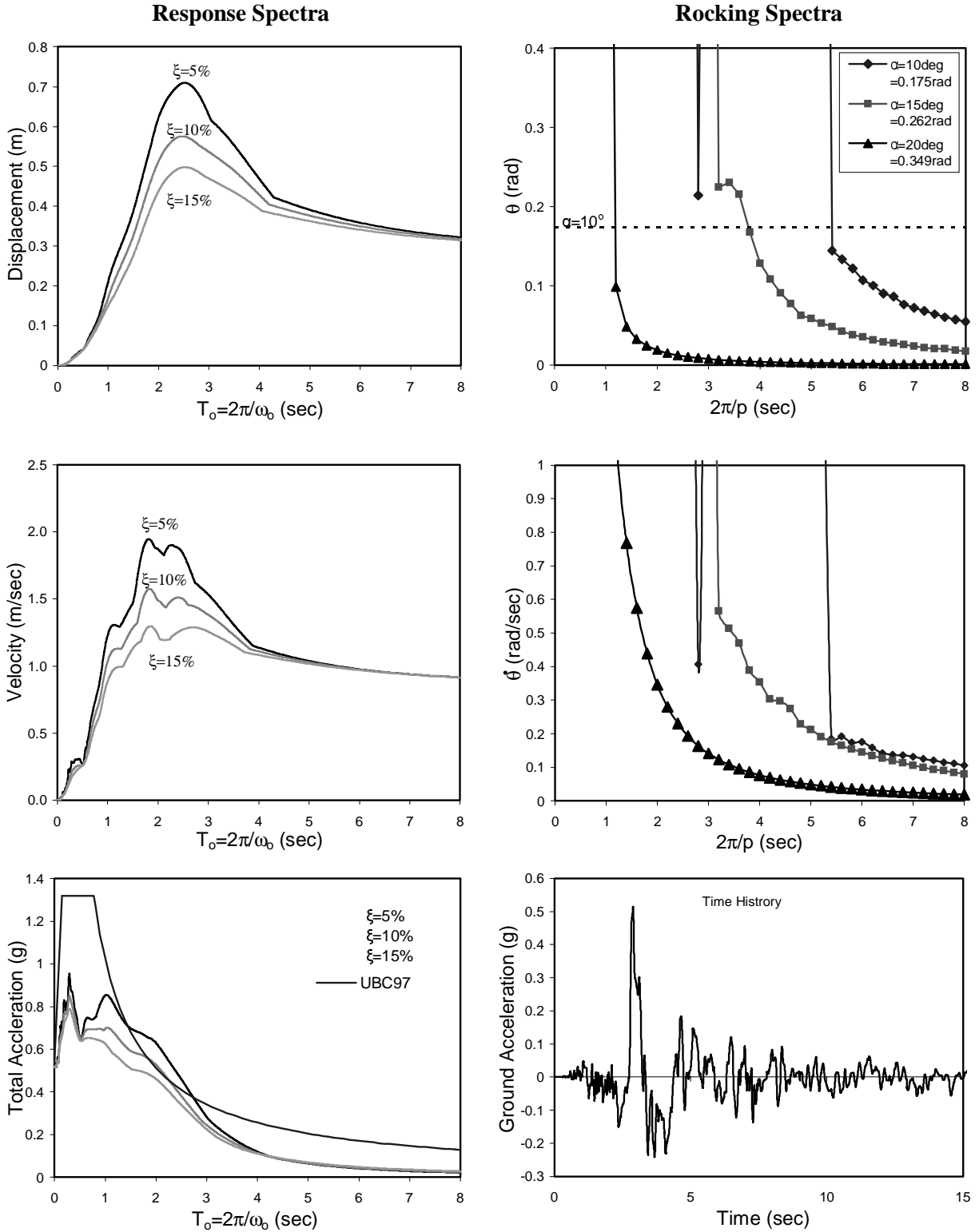


**Figure 5.6** True response spectra of a linear viscously damped oscillator (left) and rocking spectra of a rigid slender block (right) when subjected to 1992 Erzinkan, Turkey, earthquake.

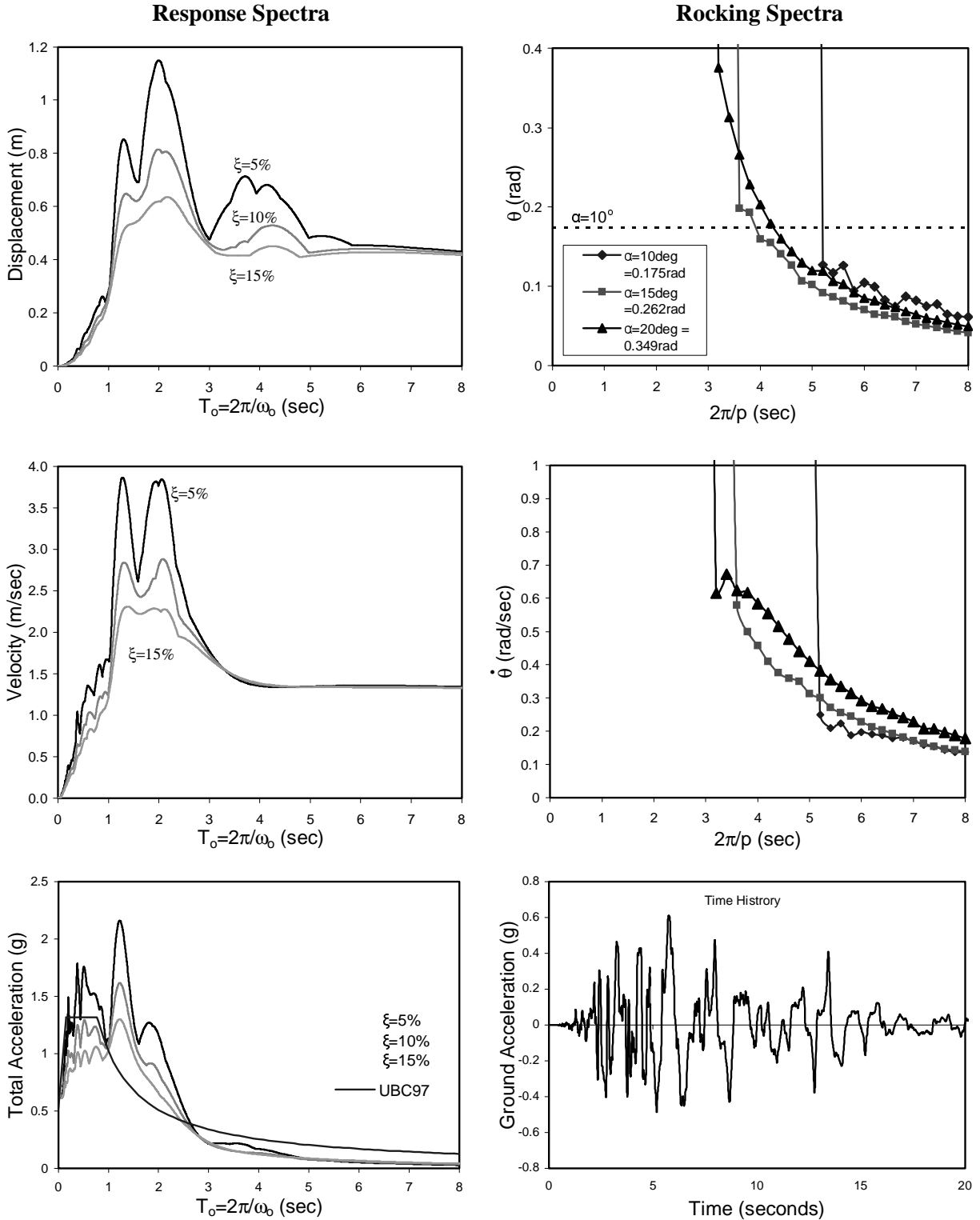


**Figure 5.7** True response spectra of a linear viscously damped oscillator (left) and rocking spectra of a rigid slender block (right) when subjected to the Takatori motion recorded during the 1995 Kobe, Japan, earthquake.

## 6 A New Measure of Earthquake Shaking

Before examining the shortcomings that result from the superficial analogy between the response of a SDOF structure and a rocking block, this section elaborates on some interesting observations which indicate that the rocking spectra can be used as a supplemental measure of earthquake shaking which complements the valuable information that one draws from the response spectra.

Figure 5.1 (right) indicates that any block with slenderness  $\alpha=10^\circ$  that is small enough so that  $2\pi/p < 4$  [ $R < 2.98\text{m}$  (117.3'')] will overturn when subjected to the Pacoima Dam record. Less slender blocks experience smaller rotations and are in principle more stable. For instance, a block with slenderness  $\alpha=20^\circ$  will survive the Pacoima Dam record even if it is as small as  $2\pi/p=2$  [ $R=0.74\text{m}$  (29.3'')]. Larger blocks, say  $2\pi/p > 6$  [ $R > 6.71\text{m}$  (264.0'')], will uplift, but the maximum rotation is only a fraction of their slenderness,  $\alpha$ , even for the strong ground motions with PGA/g more than four times the slenderness of a block with  $\alpha=15^\circ$  (See Table 5.1). Figure 5.2 (right) shows rocking spectra from the fault-normal component of the Array #5 motion recorded during the 1979 Imperial Valley earthquake that has a PGA/g 0.379, which is slightly larger than the value of  $\tan(20^\circ)=0.364$ .

When comparing the response and rocking spectra shown in Figures 5.1 and 5.2, one can make several interesting observations in conjunction with the kinematic characteristics of the ground motions offered in Table 5.1. Indeed the rotations induced by the Array #5 record to blocks with slenderness  $\alpha=20^\circ$  are minimal (close to zero) whereas the rotations induced by the

Pacoima Dam record (more than three times larger PGA) to blocks with  $\alpha=20^\circ$  are appreciable (in particular for  $2\pi/p < 6$ ).

The rotations induced by the Array #5 record to blocks with slenderness  $\alpha=15^\circ$  are comparable to the rotations induced to the same blocks by the Pacoima Dam record; smaller blocks ( $2.6 \leq 2\pi/p \leq 3$ ) survive the more “gentle” Array #5 record yet topple from the more “violent” Pacoima Dam record. When observing the response of blocks with slenderness  $\alpha=10^\circ$ , the situation reverses. The Array #5 record topples every block with  $2\pi/p < 6.5$ , while blocks with  $\alpha=10^\circ$  are much more stable when subjected to the Pacoima Dam record, as every block with  $2\pi/p > 4$  survives the motion. The reason that the Array #5 record is more capable than the Pacoima Dam record to overturn slender blocks is because it contains a 3.2-sec-long type-B pulse. The significance of the duration of a long pulse in achieving overturning in association with its acceleration intensity has been discussed in depth by Makris and Roussos (2000) and Zhang and Makris (2001).

Recent studies on the shaking potential of near-source ground motions have proposed that a better indicator of the destructiveness of an earthquake might be the peak ground velocity (PGV) of the record. However, in this case, the peak ground velocity alone cannot elucidate the problem, as the Pacoima Dam record results to a higher PGV than the Array #5 record. The earthquake response of rigid blocks and its nonuniform character have been recently investigated in depth by Makris and Roussos (2000), who showed that the response of different blocks is more sensitive to the kinematic characteristics of distinct, yet different, pulses within the excitation history. In particular, a dependable indicator of the overturning potential of a ground motion is the “*incremental ground velocity*” (Bertero et al. 1978—that is the net increment of the ground

velocity along a monotonic segment of its time history) in association with the duration of the local distinguishable pulse.

The response spectra of the Pacoima Dam record and the Array #5 record also exhibit noticeable differences but of a different nature. For instance, up to  $T_o \approx 1.7\text{sec}$ , the Pacoima Dam record results to higher spectral displacements than the Array #5 record. However, at  $T_o=4\text{sec}$ , the Array #5 record results to spectral displacements more than two times the spectral displacements that result from the Pacoima Dam record. Nevertheless, this behavior is uniform for all three values of damping,  $\zeta=5\%$ ,  $10\%$ , and  $15\%$ , contrary to the case of rocking spectra for which the behavior is nonuniform for different values of slenderness (damping).

Figure 5.3 (right) shows the rocking spectra for the Los Gatos motion, recorded during the 1989 Loma Prieta earthquake. The interesting element of these spectra is that they show isolated examples where (a) a small block can survive the motion that overturns a larger block (see spectra for  $\alpha=10^\circ$ ) and (b) a more slender block can survive the motion that overturns a less slender block (see where spectra for  $\alpha=15^\circ$  and  $\alpha=20^\circ$  cross).

Figures 5.4 and 5.5 reveal similar trends to those observed and discussed in Figures 5.1 and 5.2. For instance, the  $\alpha=20^\circ$  rotation spectrum of the Rinaldi record (Figure 5.4) exceeds the  $\alpha=20^\circ$  rotation spectrum of the Sylmar record (Figure 5.5), whereas the  $\alpha=10^\circ$  rotation spectrum of the Rinaldi record yields smaller values and is more stable than the  $\alpha=10^\circ$  rotation spectrum of the Sylmar record.

Another interesting observation in the spectra of the Sylmar record is that while the displacement spectra for different values of damping ratio show minor differences beyond  $T_o=4$  sec, the rotation spectra show dramatic differences even for values of  $2\pi/p=8$  sec. This trend is also observed with nearly identical pattern in Figure 5.6, which shows the response and rocking

spectra of the 1992 Erzinkan, Turkey, earthquake. In contrast, the rotation spectra of the Takatori motion, 1995 Kobe, Japan (Figure 5.7), show relatively small differences beyond the value of  $2\pi/p=5$  sec. In conclusion, this section highlights the following two observations which uncover major differences in the trends of the response and rocking spectra:

- (a) When for a prescribed value of viscous damping, a response spectrum of a given earthquake exceeds the response spectrum of another earthquake, the same will happen (with few local exceptions) for a different value of viscous damping. Contrarily, when for a prescribed slenderness, the rocking spectrum of a given earthquake exceeds the rocking spectrum of another earthquake, it is not guaranteed that the same will happen for a slightly different value of the slenderness.
- (b) There are period ranges where the values of the displacement spectra are nearly insensitive to the value of viscous damping ratio  $\xi$ . However, the rotation (uplift) spectra are very sensitive to the value of slenderness  $\alpha$  throughout the  $2\pi/p$  range.

The abovementioned differences have been the main motivation for proposing the use of the rocking spectrum as a complementary tool to the response spectrum in order to quantify the shaking potential of a ground motion.

## 7 Free Vibrations of Rocking Block

The rocking motion of a rigid block is an inherently nonlinear problem. Nonlinearities emerge from several sources and become dominant when the rotation of the block,  $\theta$ , approaches or exceeds its slenderness  $\alpha$ . For instance, Makris and Zhang (1999) and Zhang and Makris (2001) have shown that the overturning of a rigid block is a *multivalued* problem since a rigid block can survive a ground acceleration that exceeds the first ground acceleration which is capable of overturning it. This multivalued and nonlinear response exists even for very slender blocks, and the abovementioned references have shown that there is a frequency range where equations (4.1) and (4.2) cannot be linearized even for small values of the slenderness  $\alpha$ .

During a free-vibration regime that does not result in toppling (say with initial conditions  $\theta_o < \alpha$  and  $\dot{\theta}_o = 0$ ), the situation is simpler than during a forced-vibration regime, and the equations of rocking motion can be linearized with confidence for slender blocks (about  $\alpha \leq 20^\circ$ )

$$\ddot{\theta}(t) - p^2\theta(t) = p^2\alpha \quad \theta < 0 \quad (7.1)$$

$$\ddot{\theta}(t) - p^2\theta(t) = -p^2\alpha \quad \theta > 0 \quad (7.2)$$

The linearized pair of equations given by (7.1) and (7.2) can be easily integrated analytically,

$$\theta(t) = A_1 \sinh(pt) + A_2 \cosh(pt) - \alpha \quad \theta < 0 \quad (7.3)$$

$$\theta(t) = A_3 \sinh(pt) + A_4 \cosh(pt) + \alpha \quad \theta > 0 \quad (7.4)$$

where  $A_1$  to  $A_4$  are integration constants that are determined at the initiation of each segment of the response (Makris and Roussos 2000). The solution given by Equations (7.3) and (7.4) reveals that the free-vibration response of the rocking block is described by *hyperbolic* sines and cosines and *not* by *harmonic* (trigonometric) functions. This fundamental difference has been the motivation to avoid the term “oscillations” for the free-vibration response of a rocking block in this report.

The free-vibration response of the rocking block at its linear limit was investigated by Housner (1963), who was able to derive a relation between the maximum rotation after the  $n^{\text{th}}$  impact,  $\theta_n$ , and the initial rotation,  $\theta_o$ ,

$$\frac{\theta_n}{\alpha} = 1 - \sqrt{1 - r^n \left[ 1 - \left( 1 - \frac{\theta_o}{\alpha} \right)^2 \right]} \quad (7.5)$$

where  $r$  is the coefficient of restitution given by (4.8). Equation (7.5) that relates the rotation after  $m=n/2$  cycles to the initial rotation  $\theta_o$ , induces the temptation to relate its result with the so-called logarithmic decrement of the amplitude of the  $m^{\text{th}}$  cycle of a SDOF damped oscillator

$$\ln \left( \frac{u_o}{u_m} \right) = \frac{2m\pi\xi}{\sqrt{1-\xi^2}} \quad (7.6)$$

Equation (7.6) for lightly damped systems becomes

$$\xi = \frac{1}{2m\pi} \ln \left( \frac{u_o}{u_m} \right) \quad (7.7)$$

after approximating  $\sqrt{1-\xi^2}$  with one.

Priestley et al. (1978) noticed this resemblance—while downplaying the fundamental differences in the mathematical structure of the response of the two systems (see Table 5.2 and Equations 7.3 and 7.4)—and proposed that since there is an apparent correspondence between

the displacement,  $u$ , of a SDOF oscillator and the rotation,  $\theta$ , of a rocking block, one can define an equivalent viscous damping ratio for the rocking block

$$\beta = \frac{1}{n\pi} \ln \left( \frac{\theta_o}{\theta_n} \right) \quad (7.8)$$

since in  $m$  cycles the block has experienced  $n=2m$  impacts (see free-vibration response in Figures 4.1 and 4.2 that happens after the expiration of the Type-B pulse). Replacing (7.5) into (7.8) gives

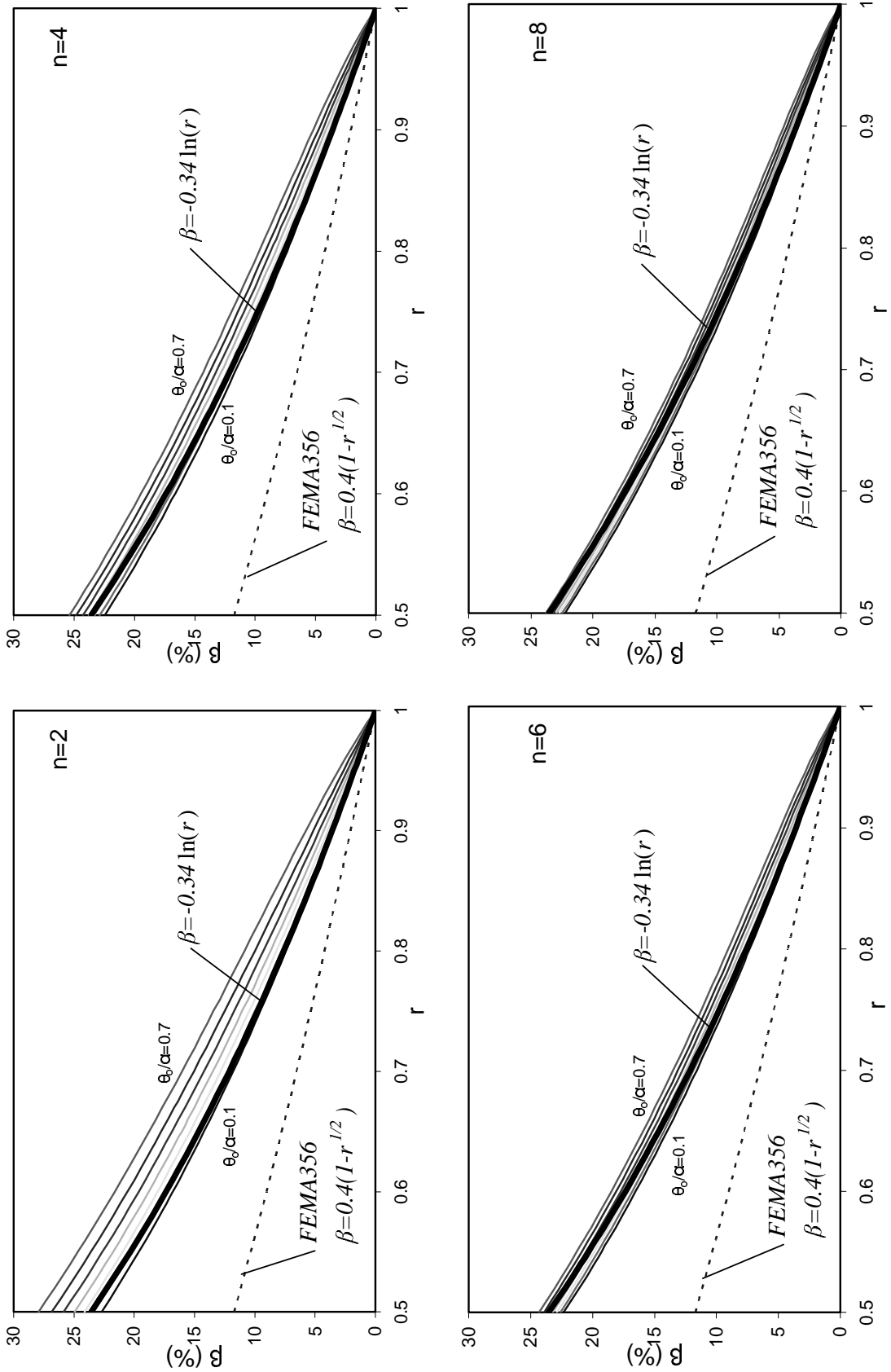
$$\beta = \frac{1}{n\pi} \ln \left\{ \frac{\theta_o}{\alpha} \frac{1}{1 - \sqrt{1 - r^n \left[ 1 - \left( 1 - \frac{\theta_o}{\alpha} \right)^2 \right]}} \right\} \quad (7.9)$$

Figure 7.1 plots the relation between the equivalent viscous damping ratio,  $\beta$ , and the coefficient of restitution,  $r$ , as results from Equation (7.9) for values of initial rotation  $\theta_o/\alpha=0.1$  to 0.7 and for four values of the number of impacts,  $n=2, 4, 6,$  and 8. As Priestley et al. (1978) indicated, this relation is comparatively insensitive to the initial rotation,  $\theta_o/\alpha$ , and number of impacts,  $n$ , and an average relation between  $\beta$  and  $r$  can be proposed that is independent of  $\theta_o/\alpha$  and  $n$ . An empirical equation that approximates this relation is

$$\beta = -0.34 \ln(r) \quad (7.10)$$

and its performance is shown with a heavy line in each quarter of Figure 7.1. The results of Equation (7.10) are very close to the graphical relation shown in Figure 3 of the Priestley et al. (1978) paper which indicates that values of the equivalent viscous damping ratio,  $\beta$ , will vary

from this relationship by less than 10% for values of  $\theta_o/\alpha \leq 0.5$  for  $n \leq 16$ . While the Priestley et al. (1978) reasoning and the results shown in Figure 7.1 appear reasonable to the nonspecialist engineer, attention is redirected to Figure 4.1 that illustrates the divergent nature of the hyperbolic functions appearing in the free-vibration response of the rocking block. The left column of Figure 4.1 plots the rocking response when the acceleration amplitude of the 2-sec-long cosine pulse is  $0.310g$ . Note that after the excitation pulse expires ( $t=2$  sec), the block experiences a negative rotation that reaches a maximum of  $\theta/\alpha=0.38$  and subsequently the block vibrations decay. A slightly stronger excitation,  $a_p=0.315g$  induces a much more pronounced negative rotation that reaches a maximum of  $\theta/\alpha=0.86$ . Therefore, a 1.6% change in the excitation amplitude results in approximately 125% change in the response. A minor further increase in the input results in overturning (catastrophe). In contrast to Figure 4.1, Figure 7.2 illustrates the robust behavior that is expressed by trigonometric functions. The left column of Figure 7.2 plots the oscillatory response of a SDOF oscillator with  $\omega_o=p=2$  rad/sec and  $\xi = -0.34 \ln(r) = 7.2\%$  (where  $r$  is the coefficient of restitution that corresponds to  $\alpha=15^\circ$ ) when subjected to a type-B pulse with  $a_p=0.310g$ . Figure 7.2 (center and right) shows that small amplifications of the input have a marginal effect on the response. This comparison shows from a different point of view that the concept of representing the rocking block as a single-degree-of-freedom oscillator with constant damping and amplitude-dependent period is inherently flawed.



**Figure 7.1** Equivalent viscous damping,  $\beta$ , of a rocking block as results from (a) the Priestley et al. (1978) analogy (Equation 7.9), (light solid lines); (b) the empirical Equation (7.10), (heavy solid lines); and (c) the FEMA 356 formula, (dashed line).

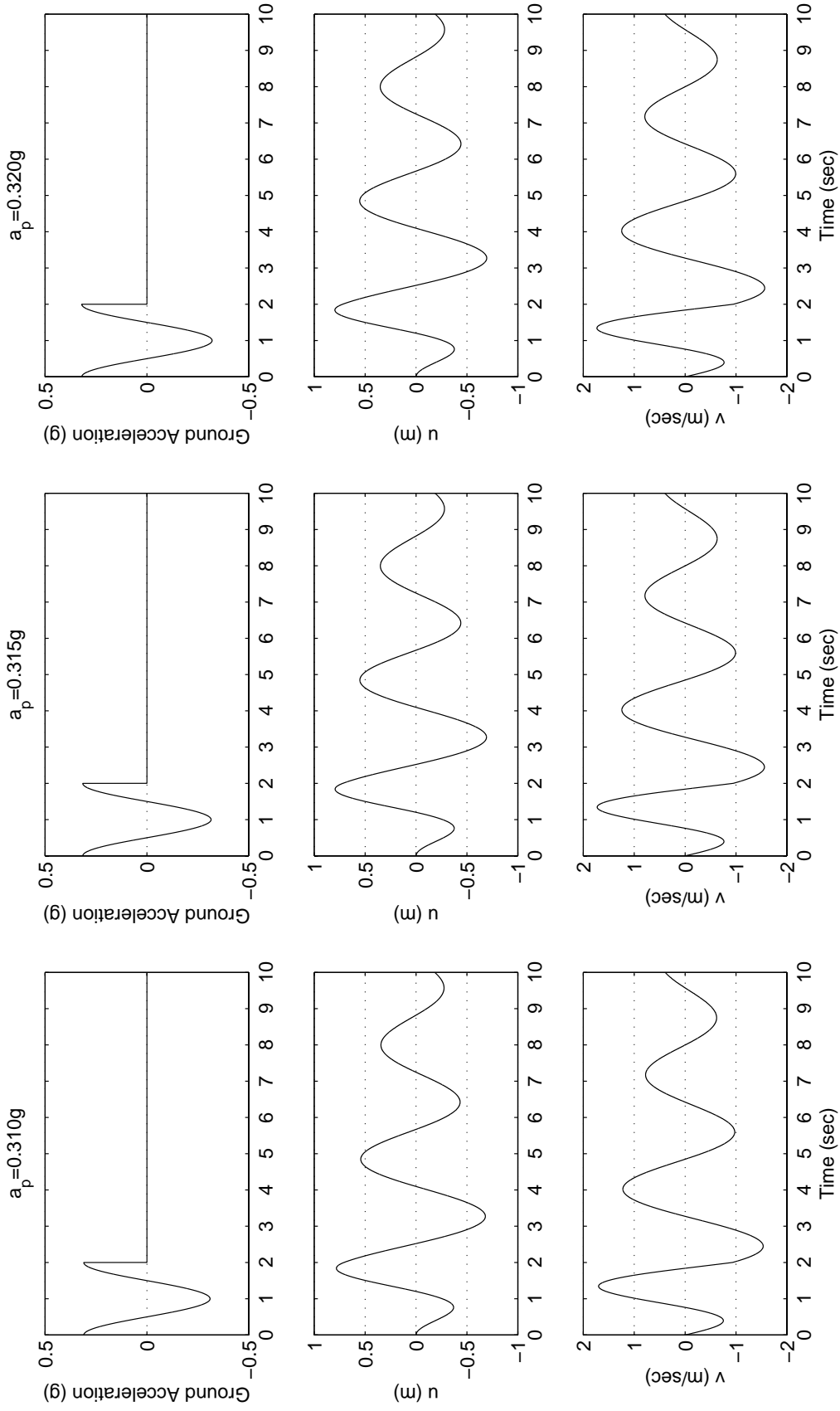


**Figure 7.2** Response of SDOF oscillator:  $\omega_o=2.0$  rad/sec,  $\xi = -0.34 \ln(0.81) = 7.2\%$ , subjected to Type-B pulse with  $T_p=2$  sec.

## 8 Estimation of Uplift Using the Response Spectra

The availability of design response spectra in association with observations from strong earthquakes motivated Priestley et al. (1978) to propose a relatively simple procedure to estimate structural displacements that originate from rocking (uplift). It includes the following steps:

- (1) Establish that the ground acceleration is strong enough to induce rocking.
- (2) Using Equation (7.5) or the graphs of Figure 7.1, estimate the equivalent viscous damping ratio,  $\xi=\beta$ , of the rocking structure.
- (3) Estimate an initial rotation  $\theta_i$  and compute the amplitude-dependent period of the rocking block from the formula derived by Housner (1963),

$$T(\theta_i) = \frac{4}{p} \cosh^{-1} \left( \frac{1}{1 - \frac{\theta_i}{\alpha}} \right) \quad (8.1)$$

- (4) From a displacement response spectrum (or even a displacement design spectrum) constructed for the value of the equivalent damping ratio estimated in step (2), read the displacement,  $\delta_i$ , of the equivalent SDOF oscillator with period  $T(\theta_i)$ .
- (5) Compute the value of the new rotation,

$$\theta_{i+1} = \frac{\delta_i}{R \cos(\alpha)} \quad (8.2)$$

(6) Compute the new local period  $T(\theta_{i+1})$  with Equation (8.1) and repeat steps (4) and (5) until convergence results.

In this section, the abovementioned procedure is examined by comparing the converged values of the rotations,  $\theta$ , that result from the Priestley et al. (1978) design approach with the exact rocking spectra presented in this report. We concentrate on blocks with slenderness  $\alpha=10^\circ$ ,  $\alpha=15^\circ$  and  $\alpha=20^\circ$ . For these values, the equivalent viscous damping ratios according to Equation (7.10) are  $\beta=\xi=3.15\%$ ,  $7.20\%$ , and  $13.12\%$ . Figures 8.1, 8.3, 8.4, 8.6, 8.8, 8.10, and 8.11 (left columns), plot the response spectra of the seven earthquakes used in this study for the aforementioned values of viscous damping. The true displacement spectra shown in Figures 8.1, 8.3, 8.4, 8.6, 8.8, 8.10, and 8.11, are used to construct the uplift spectra for blocks with  $\alpha=10^\circ$ ,  $\alpha=15^\circ$ , and  $\alpha=20^\circ$ , according to the Priestley et al. (1978) approximate method. These uplift spectra are shown in the center column of the figures together with the exact rotation spectra. The third column of Figures 8.1, 8.3, 8.4, 8.6, 8.8, 8.10, and 8.11, plots the values of the period  $T(\theta)$  given from Equation (8.1) when evaluated with the converged values of the rotations shown in the center plots.

The center plot of Figure 8.1 indicates that for the Pacoima Dam record, the Priestley et al. (1978) method is invariably overconservative, since (a) it predicts overturning of smaller blocks that in reality survive the Pacoima Dam record and (b) it predicts substantially larger rotations for larger blocks. As an example, a typical electrical transformer has a frequency parameter  $p=2$  rad/sec and a slenderness of  $\alpha=20^\circ$ . According to the bottom-center plot, the approximate method predicts a rotation of  $\theta=0.25$  rad whereas the exact solution gives  $\theta=0.08$  rad—that is less than three times smaller. As  $2\pi/p$  increases, the predictions of the Priestley et al. (1978) method become more dependable, in particular for slender blocks. Concentrating on the

top-right graph of Figure 8.1, the approximate method indicates that for  $2\pi/p=6$  sec and  $\alpha=10^\circ$ , the converged period of rocking is approximately  $T(\theta)=5.7$  sec, whereas for  $2\pi/p=7$  sec, the converged period of rocking is  $T(\theta)=6.6$  sec. Figure 8.2 (left) plots the exact time histories of blocks with size  $2\pi/p=6$  sec (middle left) and  $2\pi/p=7$  sec (bottom left) and slenderness  $\alpha=10^\circ$ . The rocking cycles have different durations, but the general trend is that larger blocks experience smaller rotations with the corresponding cycles having smaller durations. For  $2\pi/p=6$  sec ( $R=6.71$  m), the maximum duration of one cycle is 5.25 sec, which is indeed close to the period estimated by the approximate method ( $T(\theta)=5.7$  sec). For  $2\pi/p=7$  sec ( $R=9.12$  m), the maximum duration of one cycle is 3.61 sec; that is considerably smaller than the period estimated by the approximate method ( $T(\theta)=6.6$  sec).

The Priestley et al. (1978) method is flawed because it attempts to compute rotations  $\theta(T) = \delta(T_o)/(R \cos(\alpha))$  by reading the  $\delta(T_o)$  values from the displacement spectrum that shows a behavior totally different than that of the rotation spectrum. The fact that Equation (8.1) converges at some value as  $\delta(T_o)$  gets updated has nothing to do with the actual duration of the rocking cycles. For instance, for  $2\pi/p=7$  sec and  $\alpha=20^\circ$ , the converged period shown in Figure 8.2 is approximately  $T(\theta)=2.28$  sec, whereas the maximum duration of one cycle from the exact time history is 1.38 sec. According to the bottom-center plot, the approximate method predicts a rotation of 0.05 rad, whereas the exact solution gives  $\theta=0.015$  rad.

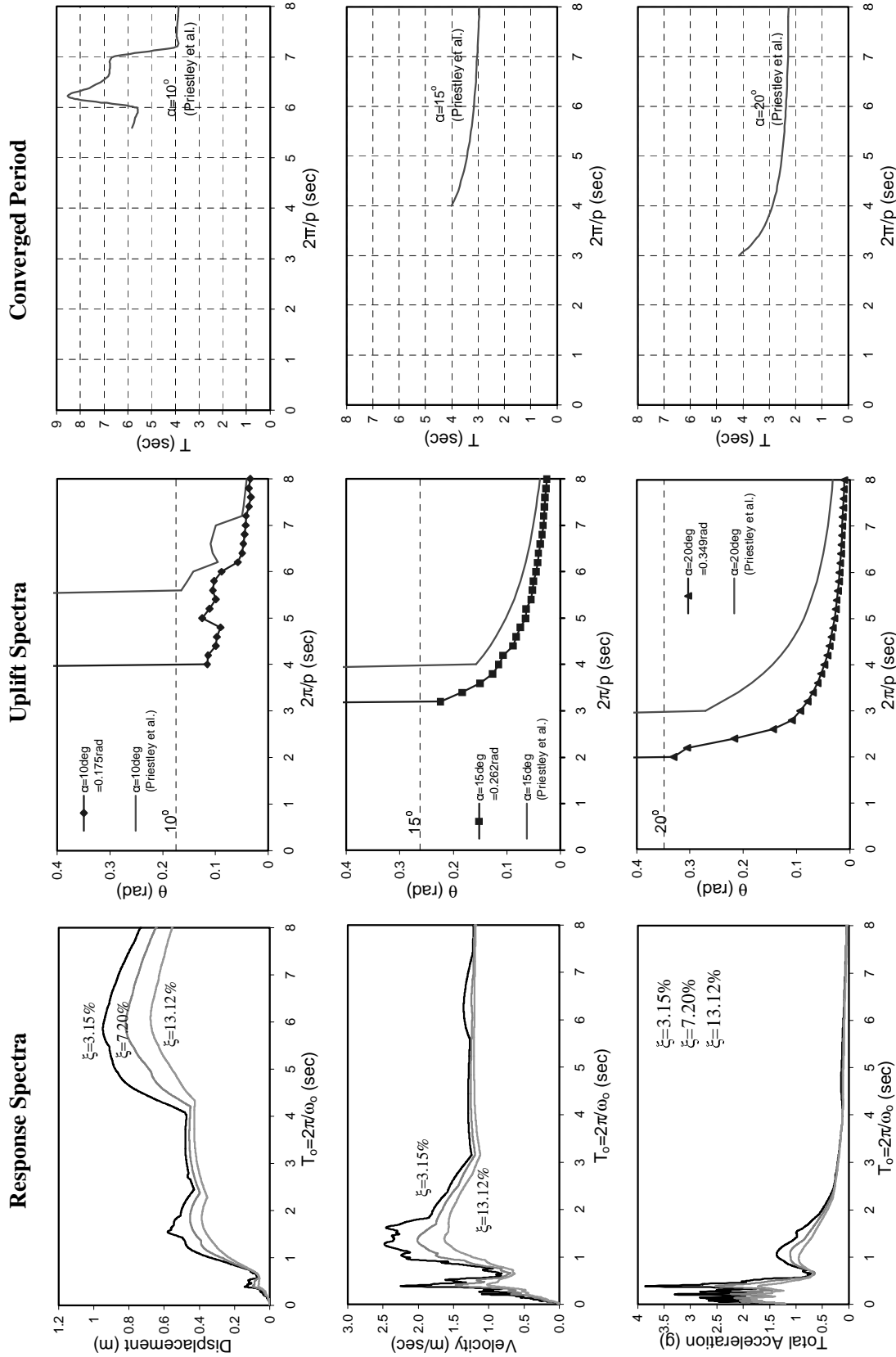
Now, the reason that the approximate spectrum assumes decreasing values as  $2\pi/p$  increases is that a nearly constant spectral displacement (see values of spectral displacement in the vicinity of  $T_o=3$  sec) is divided by an increasing  $R$  (see Equation 8.2). This has nothing to do with the mechanism of uplifting of a free-standing rigid block.

Figure 8.3 indicates that for the El Centro Array #5 record, the approximate method predicts with accuracy the rotations of large blocks with  $\alpha=10^\circ$ , while it grossly overestimates the rotations of blocks with  $\alpha=15^\circ$  and  $\alpha=20^\circ$ . A similar pattern is observed in Figure 8.4, which compares the rotation spectra of the Los Gatos record. The time histories shown in Figure 8.5 in association with the right column of Figure 8.4 offer additional evidence on the lack of correlation between the converged period  $T(\theta)$  and the actual duration of the rocking cycles.

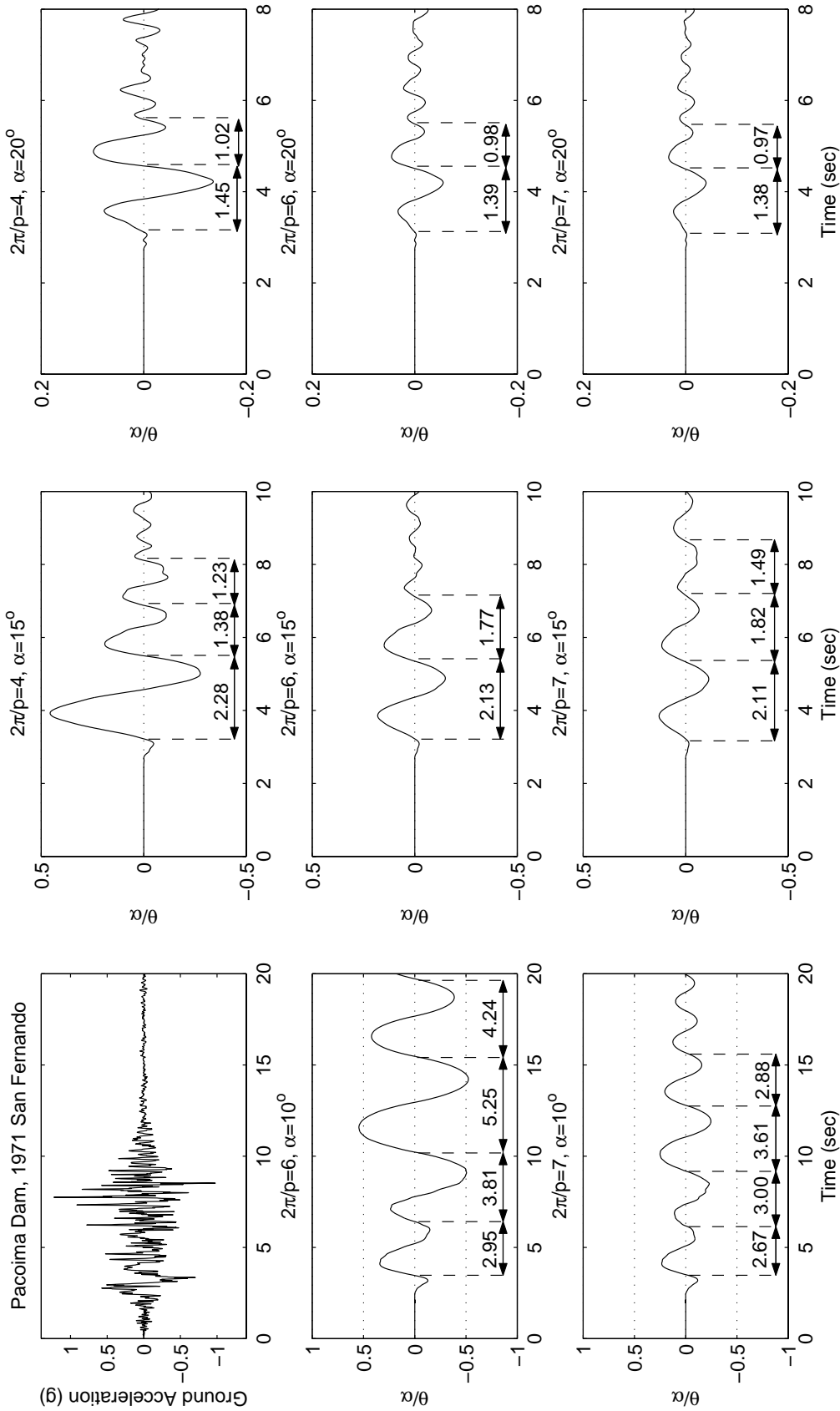
Figure 8.6 shows that for the Rinaldi record, the approximate method of Priestley et al. (1978) produces very good estimates of the rotations for all three values of  $\alpha=10^\circ$ ,  $15^\circ$ , and  $20^\circ$ . This good agreement is partly due to the unique shaking strength and morphology of the Rinaldi record. It exhibits a distinct one-second-long acceleration pulse with amplitude that reaches 0.9g. Going back to Figure 5.4 (top right), one observes that the rotations of blocks with slenderness  $\alpha=10^\circ$ ,  $15^\circ$ , and  $20^\circ$ , are crowded together in a pattern that is similar to the pattern followed by the displacement response spectrum. Furthermore, because the main pulse that dominates the response has a relative short duration (around 1 sec), the displacement response spectrum initiates its descent relatively early so that the trend followed by the displacement spectra beyond  $T_o=4$  sec resembles the trend followed by the rocking spectrum beyond  $2\pi/p=4$  sec. It is because of these unique yet accidental similarities between the response spectra and the rocking spectra that the Priestley et al. (1978) method yields such remarkably good predictions of the block rotations due to the Rinaldi motion. Figure 8.7 shows selective time histories of rocking blocks and the durations of the main rocking cycles.

Figure 8.8 shows that for the Sylmar record, the approximate method is unconservative for blocks with slenderness  $\alpha=15^\circ$  and  $\alpha=20^\circ$ . The right column of Figure 8.8 in association with Figure 8.9 indicates that for  $\alpha=10^\circ$ , the converged period of rocking is close to the actual dura-

tion of the main cycles of the rocking response. On the other hand, for  $\alpha=15^\circ$  and  $\alpha=20^\circ$ , the converged periods of rocking are substantially larger than the actual durations of the main rocking cycles. This observation confirms that the converged period computed from Equation (8.1) has nothing to do with the actual durations of the rocking cycles due to earthquake shaking. Figure 8.10 shows that for the 1992 Erzinkan, Turkey, earthquake, the predictions of the approximate method are poor, while Figure 8.11 shows that for the Takatori record (1995 Kobe, Japan), the predictions of the approximate method are surprisingly good.



**Figure 8.1** Comparison of exact and approximate uplift spectra (center column) that have been computed with the Priestley et al. (1978) method using the true displacement response spectrum (top left). The converged period that corresponds to the estimated uplift is shown in the right column. Ground Motion: Pacoima Dam, 1971 San Fernando.



**Figure 8.2** Selected time histories and durations of rocking cycles of rigid blocks with slenderness,  $\alpha=10^\circ$  (left),  $\alpha=15^\circ$  (center), and  $\alpha=20^\circ$  (right) when subjected to the Pacoima Dam record.

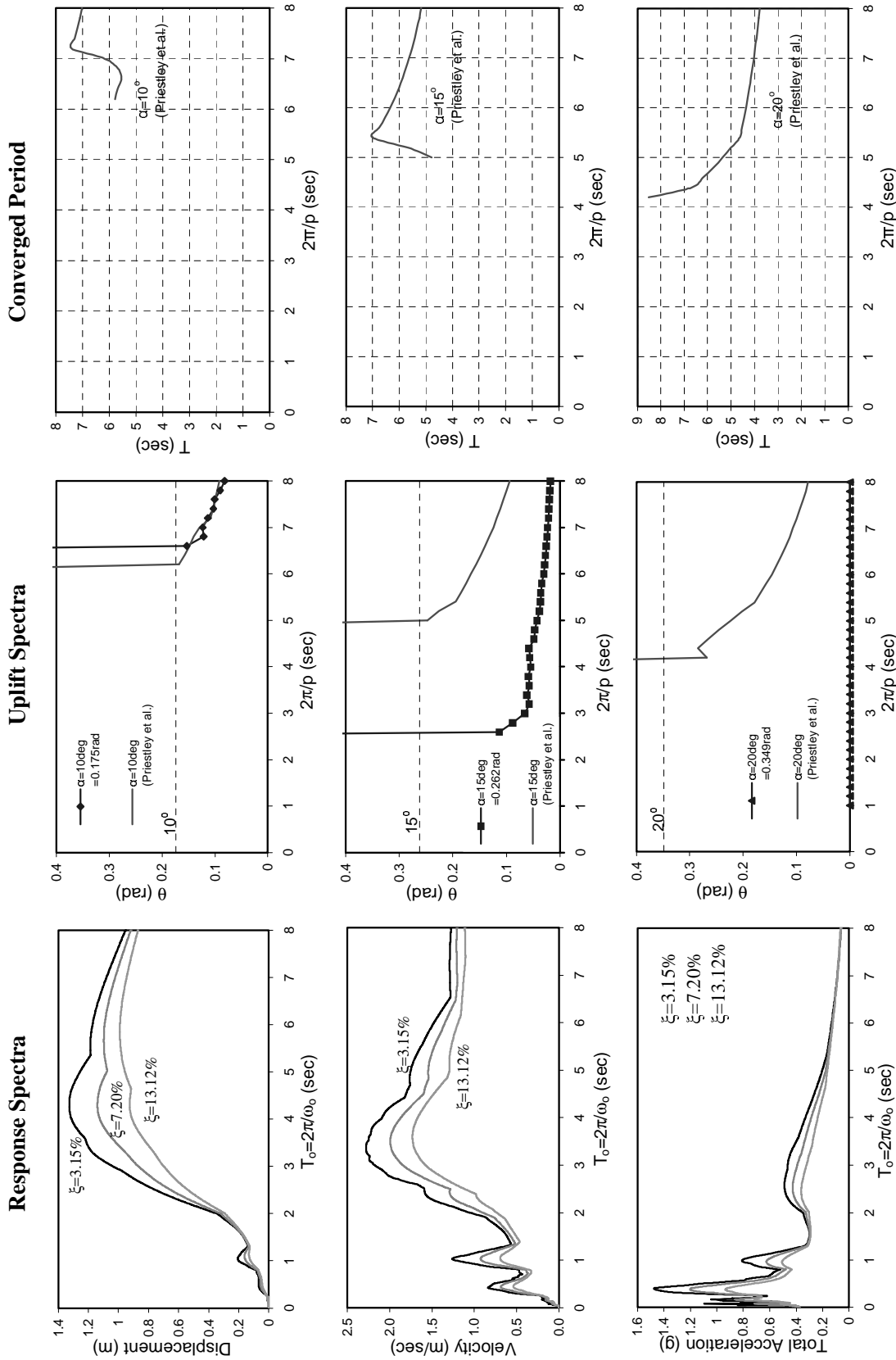


**Figure 8.3** Comparison of exact and approximate uplift spectra (center column) that have been computed with the Priestley et al. (1978) method using the true displacement response spectrum (top left). The converged period that corresponds to the estimated uplift is shown in the right column. Ground Motion: El Centro Array #5, 1979 Imperial Valley.

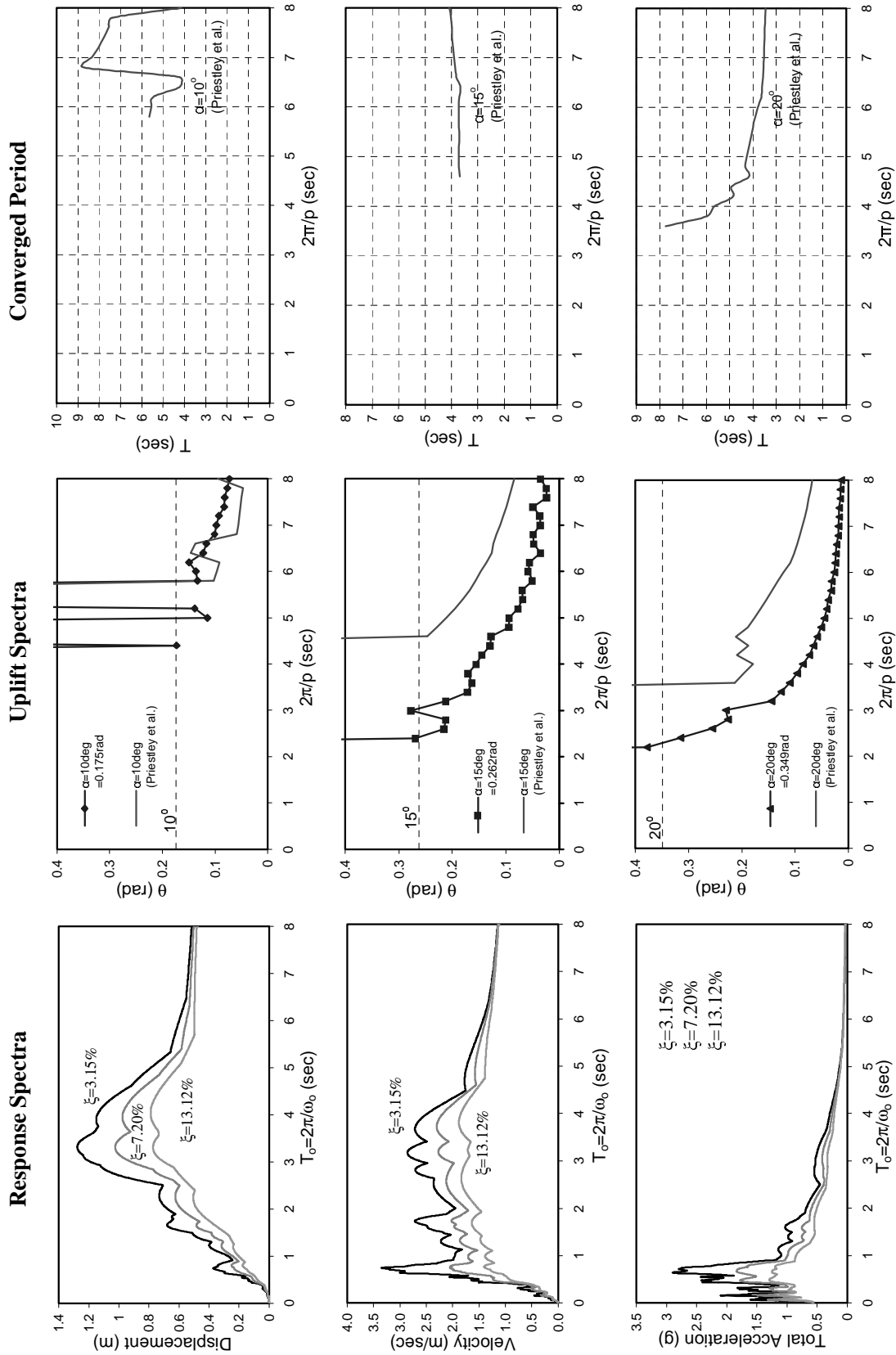


**Figure 8.4** Comparison of exact and approximate uplift spectra (center column) that have been computed with the Priestley et al. (1978) method using the true displacement response spectrum (top left). The converged period that corresponds to the estimated uplift is shown in the right column. Ground Motion: Los Gatos, 1989 Loma Prieta.

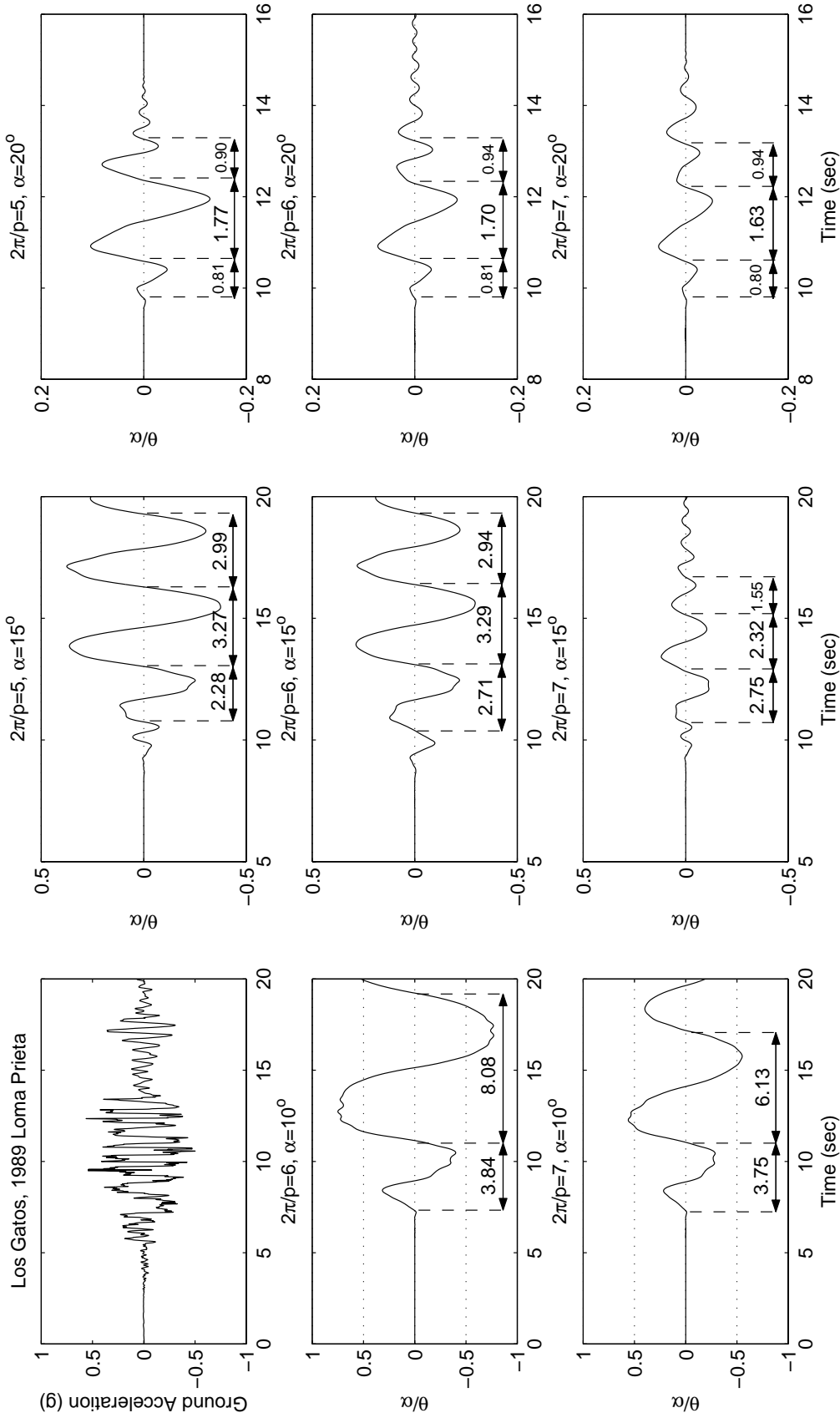


**Figure 8.5** Selected time histories and durations of rocking cycles of rigid blocks with slenderness,  $\alpha=10^\circ$  (left),  $\alpha=15^\circ$  (center), and  $\alpha=20^\circ$  (right) when subjected to the Los Gatos record.

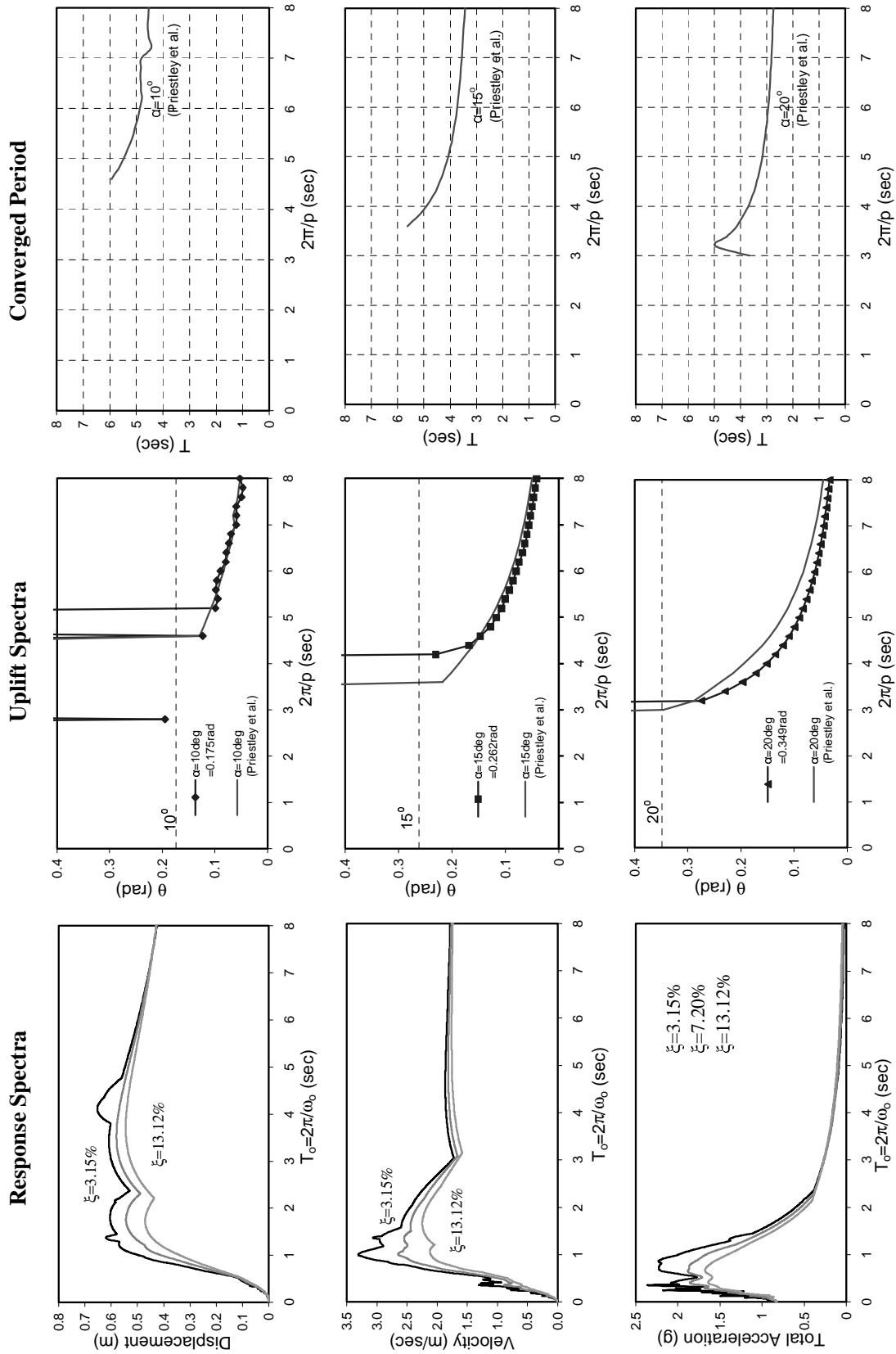


**Figure 8.6** Comparison of exact and approximate uplift spectra (center column) that have been computed with the Priestley et al. (1978) method using the true displacement response spectrum (top left). The converged period that corresponds to the estimated uplift is shown in the right column. Ground Motion: Rinaldi, 1994 Northridge.

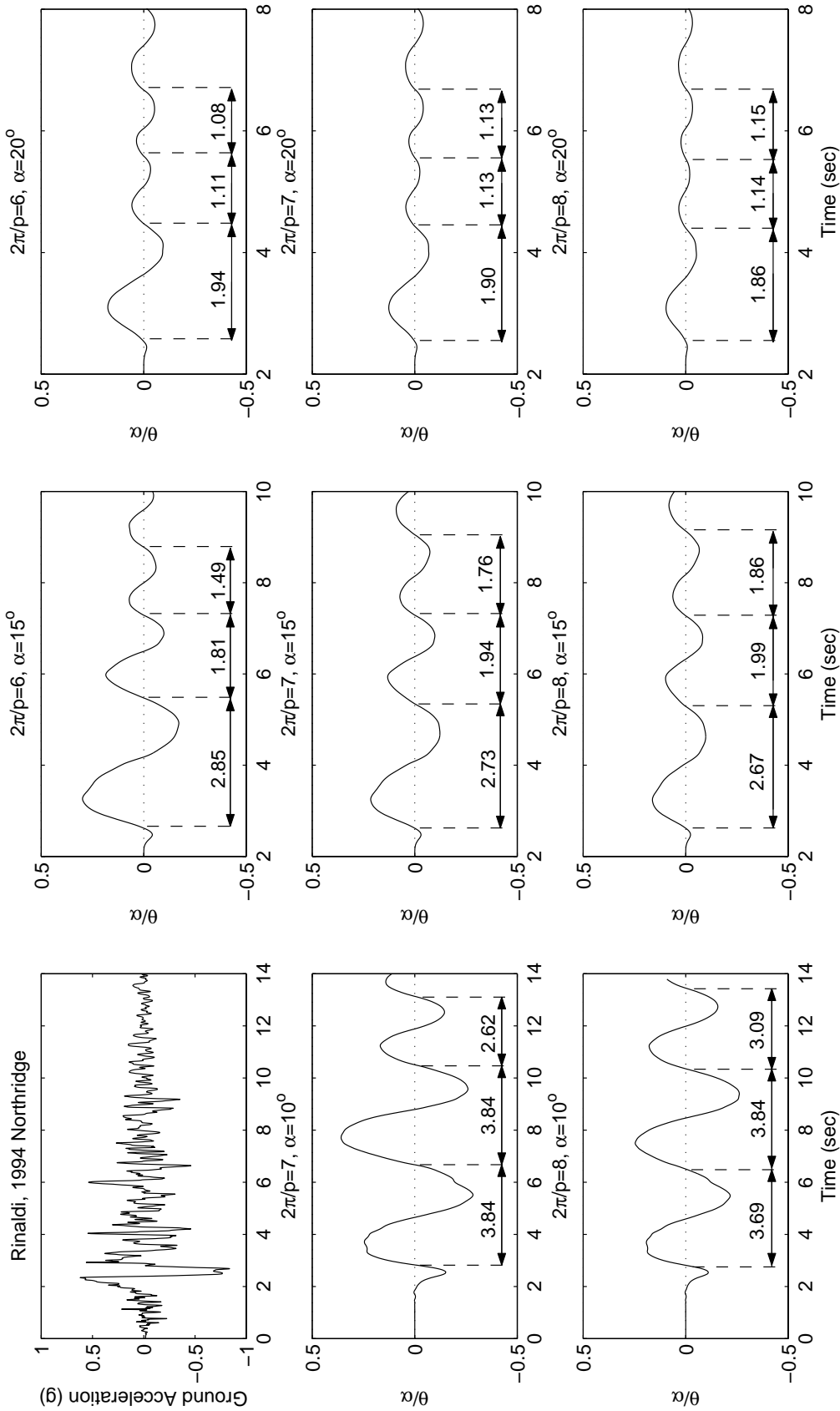


**Figure 8.7** Selected time histories and durations of rocking cycles of rigid blocks with slenderness,  $\alpha=10^\circ$  (left),  $\alpha=15^\circ$  (center), and  $\alpha=20^\circ$  (right) when subjected to the Rinaldi record.

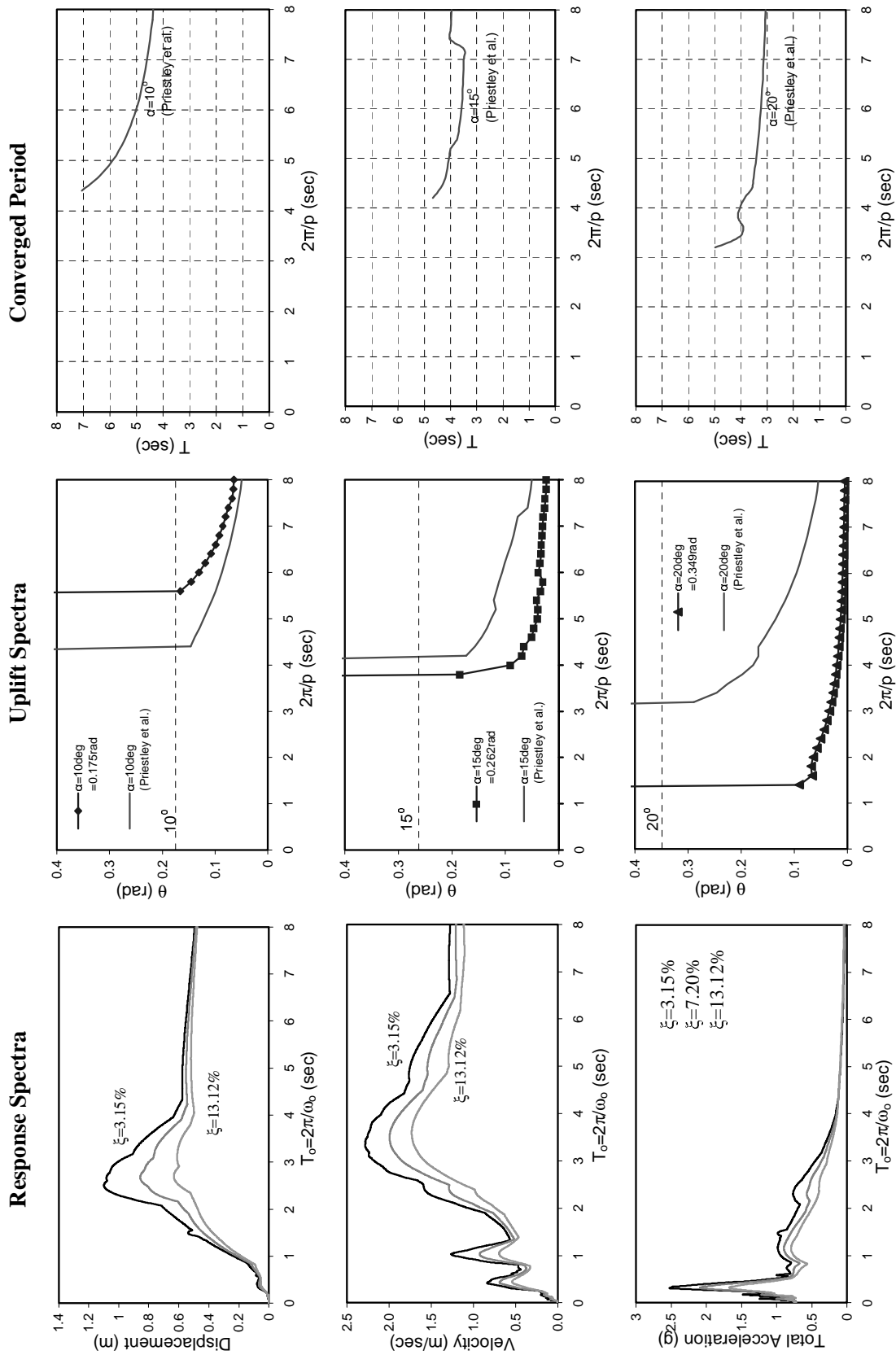


**Figure 8.8** Comparison of exact and approximate uplift spectra (center column) that have been computed with the Priestley et al. (1978) method using the true displacement response spectrum (top left). The converged period that corresponds to the estimated uplift is shown in the right column. Ground Motion: Sylmar, 1994 Northridge.

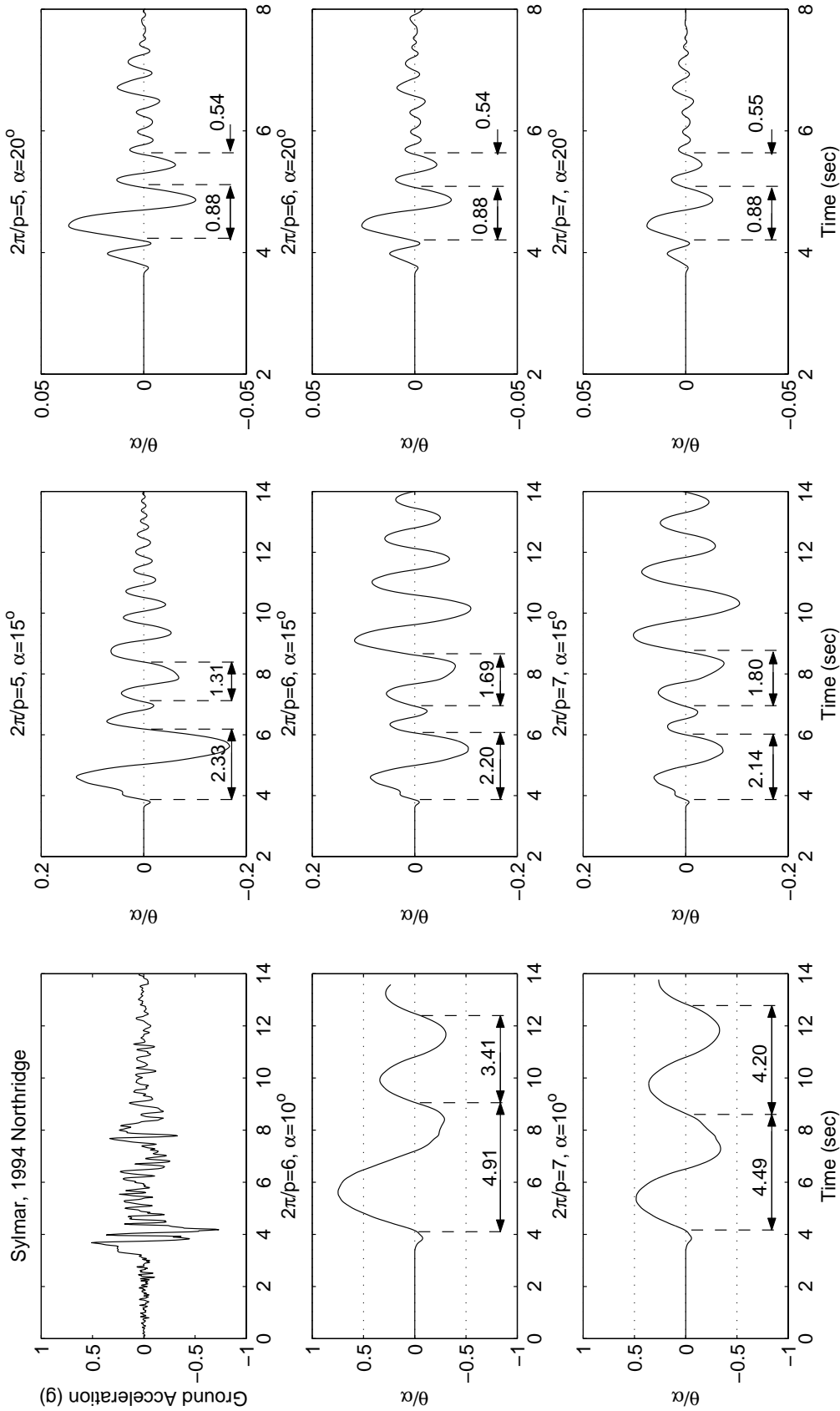


**Figure 8.9** Selected time histories and durations of rocking cycles of rigid blocks with slenderness,  $\alpha=10^\circ$  (left),  $\alpha=15^\circ$  (center), and  $\alpha=20^\circ$  (right) when subjected to the Sylmar record.

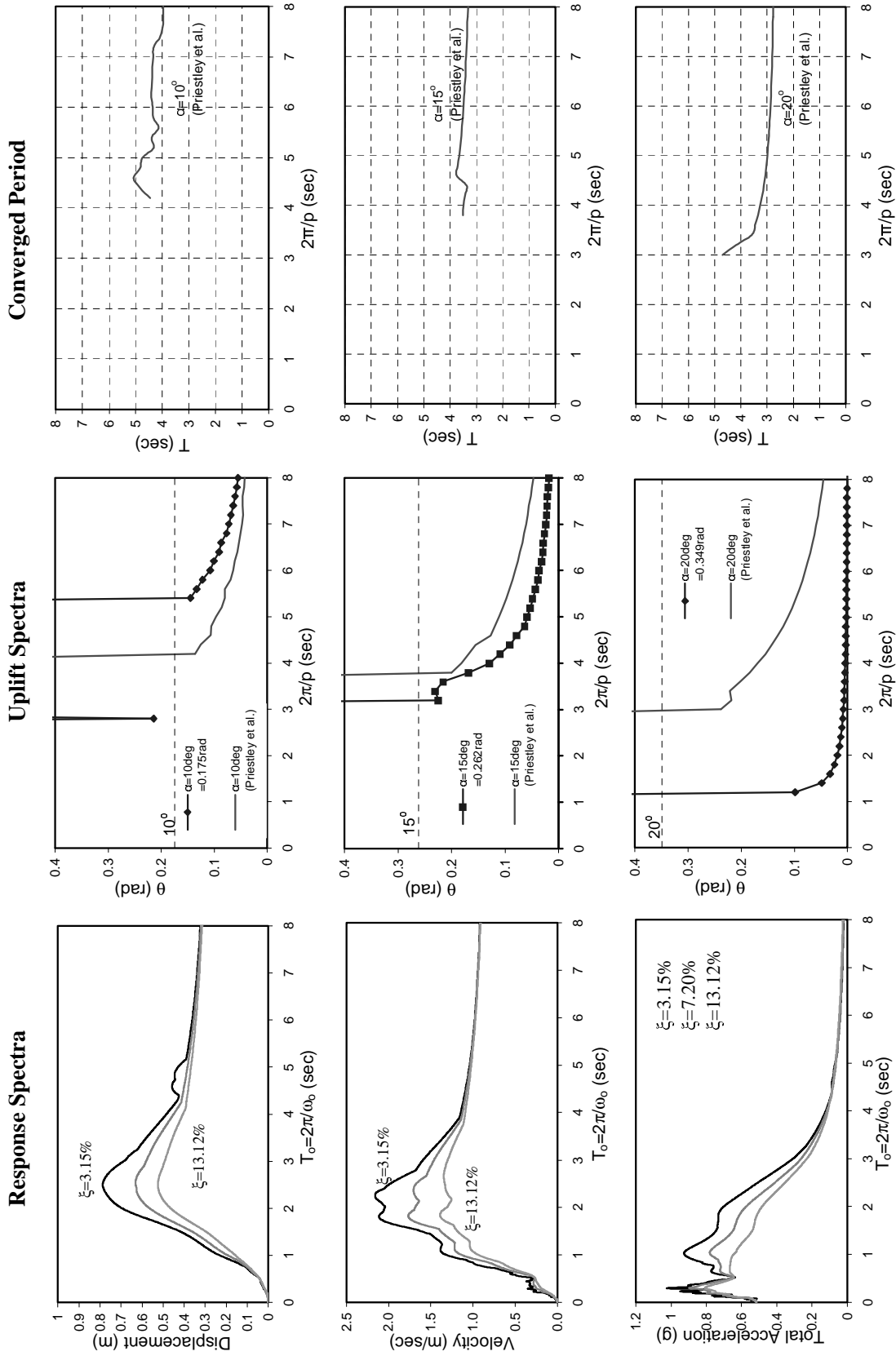


**Figure 8.10** Comparison of exact and approximate uplift spectra (center column) that have been computed with the Priestley et al. (1978) method using the true displacement response spectrum (top left). The converged period that corresponds to the estimated uplift is shown in the right column. Ground Motion: 1992 Erzincan, Turkey.

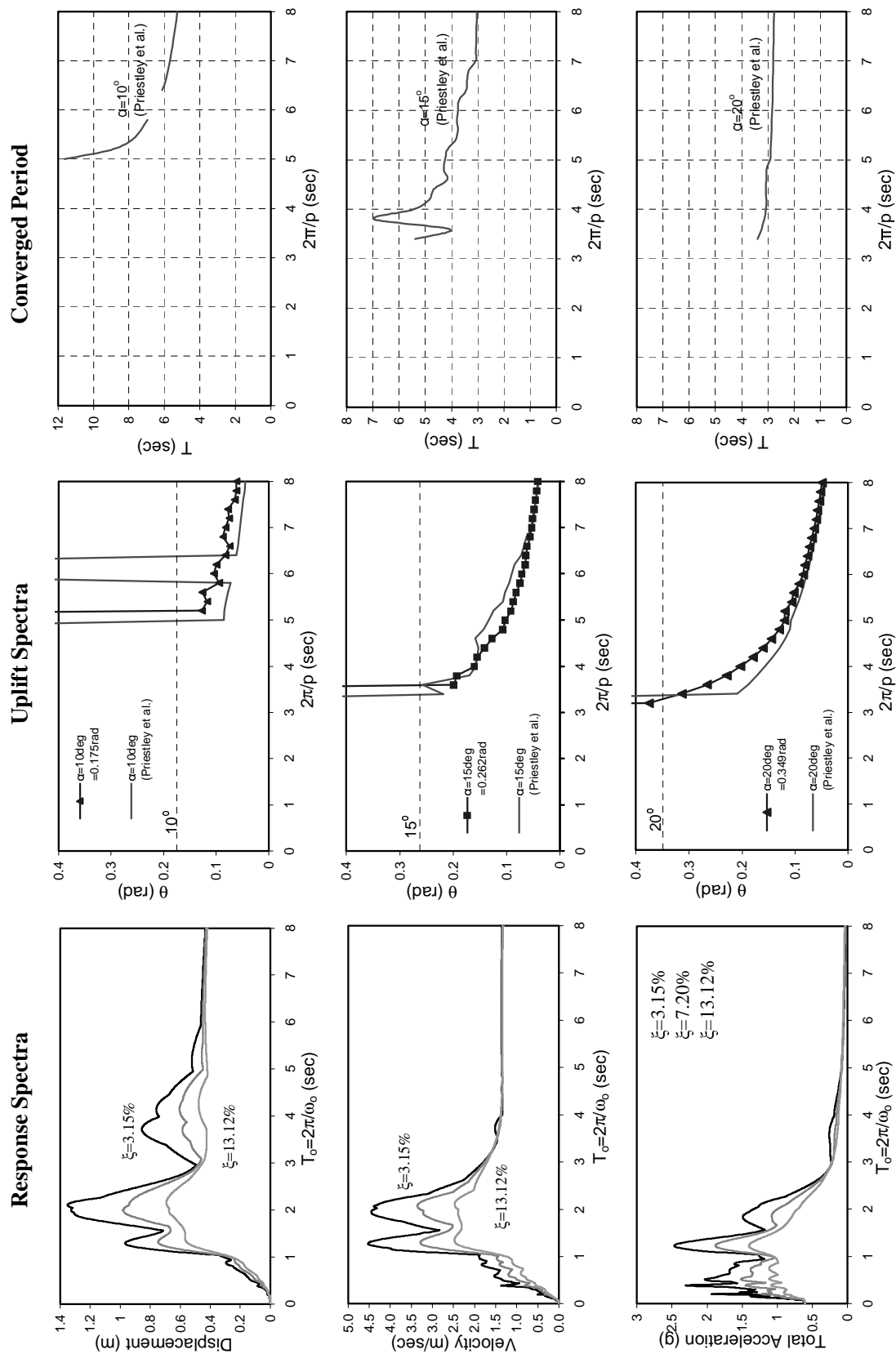


**Figure 8.11** Comparison of exact and approximate uplift spectra (center column) that have been computed with the Priestley et al. (1978) method using the true displacement response spectrum (top left). The converged period that corresponds to the estimated uplift is shown in the right column. Ground Motion: Takatori, 1995 Kobe, Japan.

## 9 The FEMA 356 Guidelines

Under the chapter “Foundation and Geologic Site Hazards,” the Federal Emergency Management Agency (FEMA) 356 document *Prestandard and Commentary for the Seismic Rehabilitation of Buildings* recommends as a possible procedure for estimating rotations of rocking structures the approximate procedure examined in the previous section of this report. The only difference in the FEMA recommendation is that instead of the exact displacement spectra (as those used in Figures 8.1, 8.3, 8.4, 8.6, 8.8, 8.10, and 8.11), one should use the FEMA design acceleration spectra (as those shown in the bottom left of Figures 5.1 to 5.7) modified for the equivalent viscous damping of the rocking block in question

$$\beta = 0.4(1 - \sqrt{r}) \quad (9.1)$$

where  $r$  is the coefficient of restitution given by Equation (4.8). The spectral displacement values needed to extract the rotations  $\theta_i$  from Equation (8.2) are obtained from Equation (3.5). For the FEMA-recommended empirical expression (9.1) that furnishes the design value of the equivalent damping ratio, we do not have information on its origin. The resulting values of  $\beta$  from Equation (9.1) are plotted in Figure 7.1 with a dashed line together with the values of  $\beta$  prescribed by Equation (7.10). It is shown that the FEMA expression yields values of  $\beta$  which are about one-half the values of  $\beta$  predicted by Equation (7.9).

Figures 9.1 and 9.2 compare the predictions of the FEMA recommendations with the exact spectra. Note that for all five U.S. earthquake motions examined in this study, the FEMA recommendation predicts overturning of all blocks with slenderness  $\alpha=10^\circ$  and as large as  $2\pi/p=8$ . For values of  $\alpha=15^\circ$  and  $\alpha=20^\circ$ , the FEMA procedure grossly overestimates rotations to the extent that they are of no use. For the Los Gatos record (right column of Figure 9.1), the FEMA guideline predicts overturning of all blocks as large as  $2\pi/p=8$  for  $\alpha=10^\circ$ ,  $\alpha=15^\circ$ , and  $\alpha=20^\circ$ . Consequently, the concept of estimating rotations of rocking blocks by using response spectra should be abandoned.

An attempt to estimate rotations of a rocking block by using response spectra of an oscillating SDOF structure resembles an attempt to find a location in the City of London by using a map of New York City. It might happen that a visitor in London is on a location that resembles New York, and by following the wrong map to guide himself accidentally to the right place. Most probably as his visit unfolds, he will be totally lost.

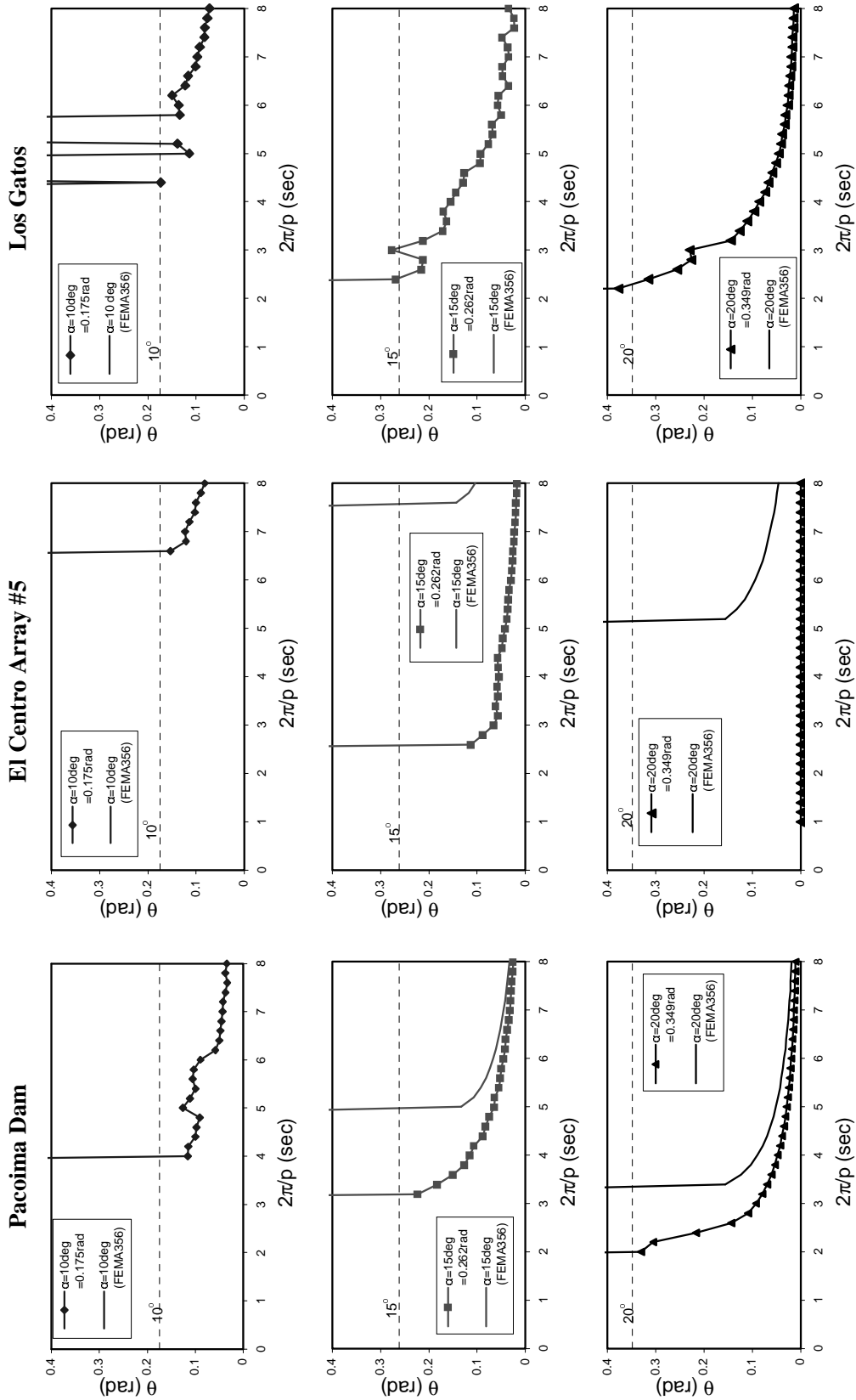
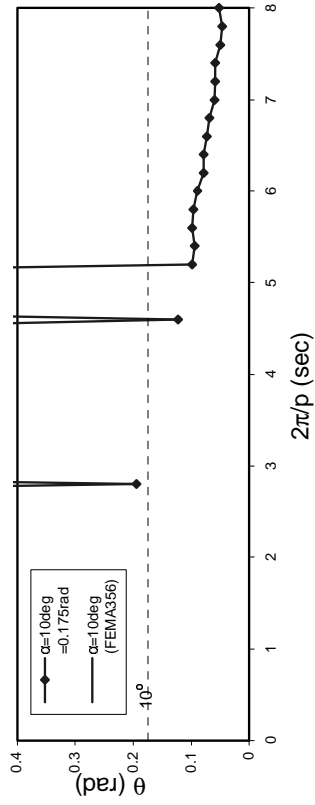


**Figure 9.1** Comparison of exact and design uplift spectra that have been computed with the Priestley et al. (1978) method using the FEMA design displacement spectra. When the solid line is not shown, the FEMA procedure predicts overturning over the entire  $2\pi/p$  range shown.

### Rinaldi



### Sylmar

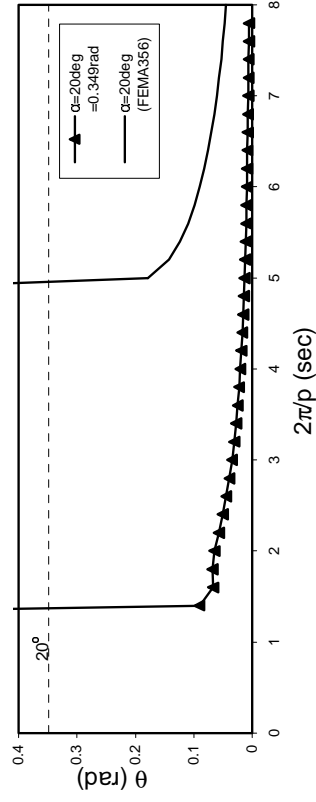
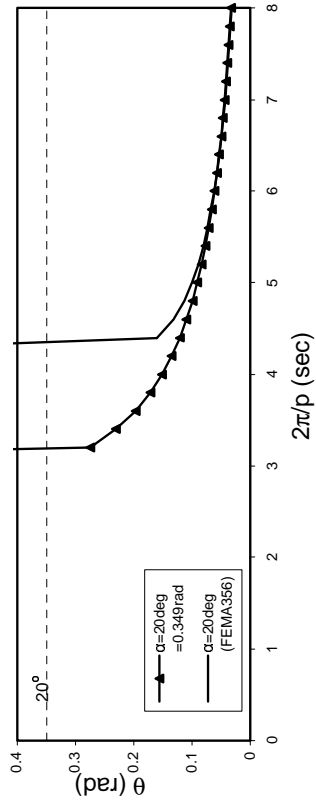
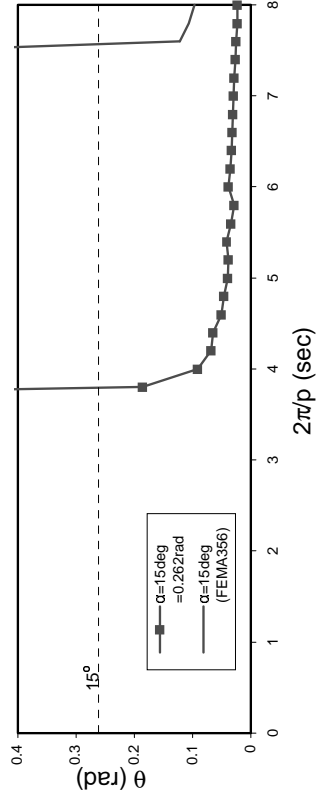
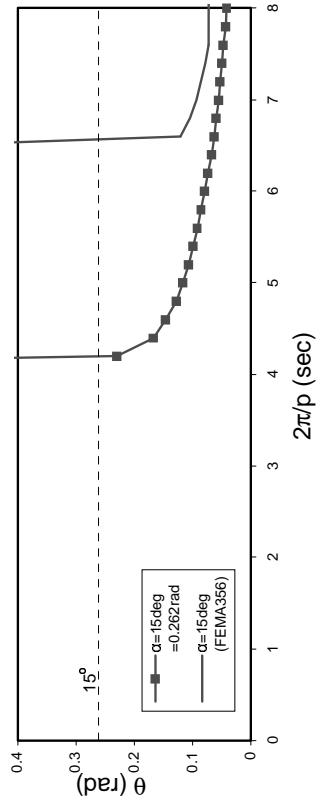
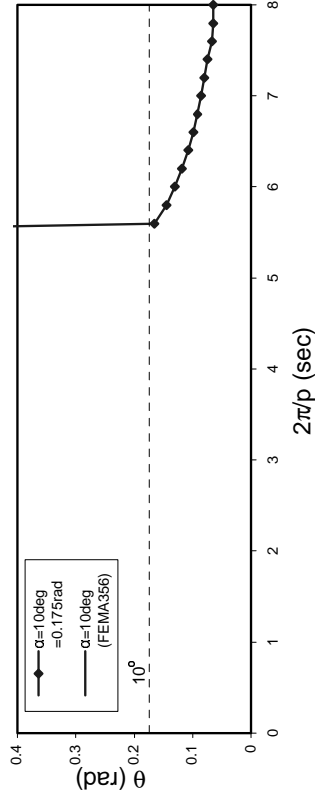


**Figure 9.2** Comparison of exact and design uplift spectra that have been computed with the Priestley et al. (1978) method using the FEMA design displacement spectra. When the solid line is not shown, the FEMA procedure predicts overturning over the entire  $2\pi/p$  range shown.

## 10 Conclusions

This report examines in depth the fundamental differences between the oscillatory response of a single-degree-of-freedom (SDOF) oscillator (regular pendulum) and the rocking response of a slender rigid block (inverted pendulum). Differences have been identified and discussed at several levels, including the form of the governing equations and the structure of the responses of the two systems.

Initially the report examines the underlying differences in the restoring mechanisms, stiffness, and damping values of the SDOF oscillator and the rocking block. Subsequently, the report proceeds by examining the differences appearing in the free- and forced-vibration response of the two systems by emphasizing the nonlinear nature and sensitivity of the dynamic response of the rocking block. It is concluded that the SDOF oscillator and the rocking block are two fundamentally different dynamical systems, and the response of one should not be used to draw conclusions on the response of the other. This conclusion motivated the proposal to use the rocking spectra as an additional valuable measure of the intensity of ground shaking. Together with the response spectra, the rocking spectra can provide a more lucid picture of the kinematic characteristics of ground motions and their implications on the response of structures.

The report examines in depth the validity of a two-decade-old approximate design methodology to estimate block rotations by performing iterations on the true or design displacement

response spectrum of oscillating structures. It is shown that the approximate method is fundamentally flawed and should be abandoned.

It is concluded that the exact rocking spectrum emerges as a distinct, valuable, and irreplaceable analysis and design tool.

## References

Bertero, V. V., S. A. Mahin, and R. A. Herrera. (1978). Aseismic Design Implications of Near-fault San Fernando Earthquake Records. *Earthquake Engineering and Structural Dynamics*. 6: 3142.

Chopra, A. K. (2000). *Dynamics of Structures: Theory and Applications to Earthquake Engineering*. 2<sup>nd</sup> ed. Upper Saddle River, N.J.: Prentice Hall.

Clough, R., and Joseph Penzien (1993). *Dynamics of Structures*. 2<sup>nd</sup> ed. New York: McGraw-Hill.

FEMA 356. (2000). *Prestandard and Commentary for the Seismic Rehabilitation of Buildings*. Prepared by the American Society of Civil Engineers for the Federal Emergency Management Agency. FEMA.

Hogan, S. J. (1989). On the Dynamics of Rigid Block Motion under Harmonic Forcing. *Proceedings of the Royal Society of London*. Series A, 425, pp 44176.

Housner, G. W. (1963). The Behavior of Inverted Pendulum Structures During Earthquakes. *Bulletin of the Seismological Society of America* 53(2): 40417.

Makris, N., and Y. Roussos (2000). Rocking Response of Rigid Blocks under Near-Source Ground Motions. *Géotechnique* 50(3): 24362.

Makris, N., and J. Zhang. (1999). *Response and Overturning of Anchored Equipment under Seismic Excitation*. Report No. PEER-98/05. Berkeley, Calif.: Pacific Earthquake Engineering Research Center, University of California.

Milne, J. (1885). Seismic Experiments. *Transactions of the Seismological Society of Japan* 8: 1-82.

*1997 Uniform Building Code*. Vol. 2. Ch. 16. International Conference of Building Officials, (1997).

Priestley, M. J. N., R. J. Evison, and A. J. Carr. (1978). Seismic Response of Structures Free to Rock on Their Foundations. *Bulletin of the New Zealand National Society for Earthquake Engineering*. 11(3) 14150.

Shenton, H. W., III (1996). Criteria for Initiation of Slide, Rock, and Slide-Rock Rigid-Body Modes. *Journal of Engineering Mechanics* 122(7): 69093.ASCE,.

Yim, S. C. S.; A. K. Chopra and J. Penzien (1980). Rocking Response of Rigid Blocks to Earthquakes. *Earthquake Engineering and Structural Dynamics* 8(6): 56587.

J. Zhang and Makris, N (2001). Rocking Response of Free-Standing Blocks Under Cycloidal Pulses. *Journal of Engineering Mechanics* 127(5)L 47383. ASCE.